Recurrent noncoding regulatory mutations in pancreatic ductal adenocarcinoma

Michael E. Feigin[1,2,20], Tyler Garvin[3,20], Peter Bailey[4], Nicola Waddell[5,6], David K. Chang[4,7,8,9], David R. Kelley[10], Shimin Shuai[11], Steven Gallinger[12,13], John D. McPherson[14], Sean M. Grimmond[4,6,*], Ekta Khurana[15], Lincoln D. Stein[11,16], Andrew V. Biankin[4,7,8,9], Michael C. Schatz[1,17,18] and David A. Tuveson[1,2,19]

[1]Cold Spring Harbor Laboratory, Cold Spring Harbor, NY, USA
[2]Lustgarten Foundation Pancreatic Cancer Research Laboratory, Cold Spring Harbor, NY, USA
[3]Watson School of Biological Sciences, Cold Spring Harbor Laboratory, Cold Spring Harbor, NY, USA
[4]Wolfson Wohl Cancer Research Centre, University of Glasgow, Glasgow, Scotland, UK
[5]QIMR Berghofer Medical Research Institute, Brisbane, Australia
[6]Queensland Centre for Medical Genomics, Institute for Molecular Bioscience, The University of Queensland, Brisbane, Queensland, Australia
[7]The Kinghorn Cancer Centre, Cancer Research Program, Garvan Institute of Medical Research, Darlinghurst, Sydney, Australia
[8]Department of Surgery, Bankstown Hospital, Bankstown, Sydney, Australia
[9]South Western Sydney Clinical School, Faculty of Medicine, University of NSW, Liverpool, Australia
[10]Department of Stem Cell and Regenerative Biology, Harvard University, Cambridge, MA USA
[11]Department of Molecular Genetics, University of Toronto, Toronto, Ontario, Canada
[12]Lunenfeld-Tanenbaum Research Institute, Mount Sinai Hospital, Toronto, Ontario, Canada
[13]Division of General Surgery, Toronto General Hospital, Toronto, Ontario, Canada
[14]Genome Technologies Program, Ontario Institute for Cancer Research, Toronto, Ontario, Canada
[15]Sandra and Edward Meyer Cancer Center, Institute for Computational Biomedicine, Department of Physiology and Biophysics, Weill Medical College of Cornell University, New York, NY USA
[16]Informatics and Biocomputing, Ontario Institute for Cancer Research, Toronto, Ontario, Canada
[17]Department of Computer Science, Johns Hopkins University, Baltimore, MD, USA
[18]Department of Biology, Johns Hopkins University, Baltimore, MD, USA
[19]Rubenstein Center for Pancreatic Cancer Research, Memorial Sloan Kettering Cancer Center, New York, NY, USA

[20]These authors contributed equally to this work.
Correspondence may be addressed to: MCS (mschatz@cshl.edu), DAT (dtuveson@cshl.edu)

*Present address: University of Melbourne Centre for Cancer Research, University of Melbourne, Melbourne, Australia

ABSTRACT

The contributions of coding mutations to tumorigenesis are relatively well known; however, little is known about somatic alterations in noncoding DNA. Here we describe GECCO (Genomic Enrichment Computational Clustering Operation) to analyze somatic noncoding alterations in 308 pancreatic ductal adenocarcinomas (PDAs) and identify commonly mutated regulatory regions. We find recurrent noncoding mutations are enriched in PDA pathways, including axon guidance and cell adhesion, and novel processes including transcription and homeobox genes. We identify mutations in protein binding sites correlating with differential expression of proximal genes and experimentally validate effects of mutations on expression. We developed an expression modulation score that quantifies the strength of gene regulation imposed by each class of regulatory elements, and find the strongest elements are most frequently mutated, suggesting a selective advantage. Our detailed single-cancer analysis of noncoding alterations identifies regulatory mutations as candidates for diagnostic and prognostic markers, and suggests novel mechanisms for tumor evolution.

INTRODUCTION

Pancreatic ductal adenocarcinoma (PDA) is a highly lethal malignancy with a 5-year survival rate of 6%, due to therapy resistance and late stage at diagnosis[1]. A detailed understanding of the molecular alterations underlying PDA is required to uncover mechanisms of tumorigenesis and enable development of effective therapies. Exome sequencing efforts have revealed genes (*KRAS*, *TP53*, *CDKN2A*, *SMAD4*) and pathways (Wnt/Notch, transforming growth factor-β (TGF-β□, axon guidance, cell adhesion) important for PDA progression[2,3]. However, the exome comprises less than 2% of the human genome. Whole-genome sequencing (WGS) analyses have uncovered an average somatic mutation rate of 2.64 mutations per megabase in PDA indicating that PDA tumors often carry thousands of mutations, the vast majority of which are located in noncoding regions and are completely uncharacterized.[4]

Relevance of noncoding mutations (NCMs) to cancer development was previously established with the discovery of highly recurrent mutations in the telomerase reverse transcriptase (*TERT*) promoter in sporadic and familial melanoma[5,6]. These mutations create binding motifs for ETS transcription factors and lead to increased *TERT* transcriptional activity[5,7]. Subsequent reports identified *TERT* promoter mutations in a wide-range of human tumors, including glioblastoma and hepatocellular carcinoma[8]. *TERT* promoter mutations are the most common genetic alterations in bladder cancer and correlate with recurrence and survival, demonstrating the potential of NCMs to act as clinical biomarkers[9]. NCMs have also been demonstrated to drive tumor progression from intergenic elements. Somatic mutations in a subset of T-cell acute lymphoblastic leukemia cases generate binding sites for the MYB transcription factor, creating a super-enhancer driving expression of the *TAL1* oncogene[10]. Recent analyses have pooled WGS data from multiple cancer types and hundreds of patients, identifying recurrent mutations in regulatory elements of several genes, including *TERT*[11-15]. While multi-cancer studies can identify ubiquitous cancer variants, in-depth analysis of individual cancer subtypes is required for uncovering disease-specific alterations[16].

To detect somatic NCMs in PDA, we developed a computational pipeline to analyze WGS data of 308 PDA tumors from the International Cancer Genome Consortium (ICGC)[17]. We used FunSeq2[18,19] to initiate prioritization of noncoding mutations, which revealed hundreds of thousands of noncoding somatic mutations with potential functional implications. To discriminate amongst this large number of NCMs, we developed GECCO (Genomic Enrichment Computational Clustering Operation) to identify candidate NCMs that drive differential gene

expression. This approach reduced the number of putative gene-proximal regulatory regions by three orders of magnitude to a set of high confidence calls.

Using GECCO, we identify novel recurrent mutations and interrogate expression data from matched tumors to find variants associated with changes in mRNA levels. We find significant differential expression of 16 genes associated with NCMs. For two of these genes, *PTPRN2* and *SLC12A8* we uncover previously unidentified clinical relevance in PDA. Specifically, we find that *PTPRN2* expression level is an independent prognostic variable for overall patient survival. Pathway analysis of the genes associated with recurrent NCMs identifies known and novel PDA pathways. Furthermore, we find enrichment for mutations in specific regulatory regions, suggesting that NCMs may be acted upon by selection during tumor formation. Our analysis provides a model for tumor evolution via the formation and selection for alterations in noncoding regulatory elements of specific genes as a means of control over specific biological pathways.

RESULTS

To analyze NCMs in PDA, we selected all 405 patients with WGS data from the ICGC Pancreatic Cancer Genome Project. We determined the total number of somatic single nucleotide variants (SNV) and small insertions or deletions (indels) for each patient, and retained those with mutation load no greater or less than 3 standard deviations from the mean (mean=7,937; range=1-440,471) to exclude the hyper-mutated tumors with unlocalized replication defects (**Fig. 1a, Supplementary Fig. 1**). In total, 2,248,158 SNVs/indels from 308 PDA patient samples were kept for analysis.

General features of GECCO

To discover the effect of noncoding mutations on PDA progression and patient outcome we developed the computational pipeline GECCO (**Fig. 2**). GECCO begins by selecting noncoding mutations falling within The Encyclopedia of DNA Elements[20] (ENCODE)-defined transcription factor binding peaks – hereby referred to as cis-regulatory regions (CRRs) as not all proteins profiled are transcription factors and may be part of larger regulatory complexes – and then proceeds with downstream processing in two parallel modules. We define a “CRR class” to be all CRRs that are bound by the same DNA-binding protein (*i.e.* CTBP2, with 1781 CRRs across the genome) or proteins involved in DNA-binding complexes (*i.e.* SUZ12, with

1618 CRRs across the genome). The first module of GECCO associates NCMs with proximal genes and uses permutation testing to identify highly mutated clusters that correlate significantly with changes in gene expression. The second module calculates the mutation rate of each CRR to determine which specific CRR classes are more commonly mutated in PDA.

In the second module, GECCO computes an expression modulation score (EMS) using coupled gene expression data to determine the regulatory impact of each CRR class. The EMS can be used to generate a rank sorted list of CRRs based on the strength of their relative gene regulatory impact (such that the strongest activators and repressors fall at both ends of the list). Taken together, the results generated from GECCO provide information on the impact of NCMs on the expression level of individual genes and identifies potential driver transcription factors. Finally, GECCO merges the results of both modules to perform pathway and clinical survival analysis, allowing novel insights into PDA biology and patterns of somatic mutations in cancer.

Prioritization of non-coding mutations

We first identified NCMs in the exact same genomic position in multiple patients and removed common human variants (MAF > 5% in 1000 Genome Phase I) (**Supplementary Table 1**)**.** This identified several variants reaching over 2% incidence (n ≥ 7 out of 308 patients) in the patient cohort (**Supplementary Table 1**). Among the 11 genes associated with these variants, 6 have been implicated in tumorigenesis, including *WASF3*[21], *BNC2*[22], *ELMO1*[23], *GPR98*[24], *PDE3B*[25] and *SOX5*[26]. Interestingly, 10 of 11 of these mutations were found in introns. However, none of the exactly recurrent mutations disrupted, or created, transcription factor-binding motifs (as defined by the JASPAR transcription factor binding profile database[27]) or fell within known regulatory elements. This analysis is consistent with several pan-cancer analyses that found few exactly recurrent mutations outside of the well-characterized *TERT* promoter mutations[11,12].

We extended this analysis by prioritizing NCMs by their association with functional annotations and clustering within regulatory elements. We used the FunSeq2 computational pipeline[18,19] as a high-level filter to remove common variants and identify putative somatic regulatory mutations with functional impact. One important benefit of this approach is that it relies on functional information and thus drastically reduces any biases resulting from non-homogeneous mutation rates across the genome. This initial round of filtering identified 301,596 potential somatic drivers across all 308 patients (mean=1,988; range=203-17,902) (**Fig. 1b**). 264,488 of the somatic NCMs fell within ENCODE-defined transcription factor-binding peaks, with the majority of the remaining mutations within enhancers (19,608) or DNaseI hypersensitive

sites (DHSs) (14,572) (**Fig. 1b**). We focused our analysis on the 264,488 NCMs within the ENCODE-defined CRRs. There was a direct correlation between CRR mutation rate and total SNVs (**Fig. 1c**). In contrast, no correlations between CRR mutation rate and coding mutations in *KRAS*, *TP53*, *CDKN2A*, *SMAD4*, and *ARID1A* were observed (**Supplementary Fig. 3**).

Analysis of cis-regulatory mutations

Starting with 264,488 candidate mutations, we used GECCO to focus our analysis on CRRs within 2kb of each gene (many of which overlap promoters), seeking to identify clusters of mutations in CRRs that directly impact gene expression (**Fig. 3a**). The requirement to be within 2kb of a gene excludes many distal enhancer regions but increases the likelihood that a given CRR topologically associates with, and therefore regulates, the expression of its proximal gene. The most frequently mutated CRR (17 patients, 5.52% of cohort) was in a TCF12-binding region proximal to *LHX8* (LIM homeobox 8) (**Fig. 3a**). *LHX8*, a homeobox gene and regulator of craniofacial development, modulates the Hedgehog pathway, a known regulator of PDA pathogenesis[28]. We observed a cluster of mutations in a E2F1-binding region in proximity to *BMP7* (bone morphogenetic protein 7). *BMP7* is a TGF-β family member, with pleiotropic roles in development and cancer progression[29]. GECCO did not detect any recurrent variants in the *TERT* promoter, in concordance with a previous study that failed to detect *TERT* promoter mutations in 24 PDA samples[8]. To determine if the identified NCMs were within active promoters or enhancers in pancreatic cells, we interrogated H3K4me3 and H3K27ac regions from ENCODE in pancreatic carcinoma-derived PANC-1 cells. In PANC-1 cells, 37.6% of all transcription factor-binding peaks were found within active PANC-1-predicted promoters or enhancers. In contrast, 58.9% of recurrent NCMs (>5 patients) were found within at least one PANC-1-predicted active promoter or enhancer. The CRRs with recurrent NCMs did not differ significantly in size from those lacking recurrent NCMs. Therefore, recurrent NCMs are enriched in transcriptionally active regions of the genome in pancreatic cancer cells.

We identified clusters of NCMs in regulatory regions of long intergenic non-protein coding RNAs (lncRNAs), including the oncogenic lncRNA Metastasis Associated Lung Adenocarcinoma Transcript 1 (MALAT1)[30], and in microRNAs, including the oncogenic miR-21[31] (**Fig. 3a**). To infer functional consequences of the most recurrently mutated gene-proximal CRRs, we used data from a published *in vitro* short hairpin RNA (shRNA) screen, which monitored survival in 102 cell lines, of which 13 were pancreas cancer-derived[32]. Knockdown of 6 (*LHX8*, *LMX1B*, *PAX6*, *DMRTA2, VAX2, CDH15*) of the top 15 genes was found to decrease cancer cell survival, providing potential functional relevance for these genes as cancer drivers

(**Fig. 3a**). Knockdown of two genes, *LMX1B* and *CDH15*, showed selective killing of PDA cell lines amongst all cancers, suggesting tumor-specific vulnerabilities.

To control for variable CRR size, we calculated a mutational frequency for each cluster harboring at least 5 mutations, defined as the number of mutations across all patients divided by the number of nucleotides spanning the cluster (**Fig. 3b**). The highest scoring result was an exactly recurrent mutation in the same genomic position in 5 patients, flanking the acyl-CoA oxidase-like gene *ACOXL*, a known susceptibility locus for chronic lymphocytic leukemia[33]. This mutation was not found to be within a known transcription factor-binding site as defined by JASPAR. We also identified a cluster of 5 mutations within 19 nucleotides proximal to the neuronal cell adhesion gene *NRXN3*, a regulator of glioma cell proliferation and migration[34].

While multi-cancer recurrent NCMs have been described[11,12], we lack an understanding of their mutational patterns. For example, it is unknown if NCMs cluster near the same genes that show recurrent coding mutations for a given disease. Therefore, we looked for clusters of NCMs in association with known PDA genes, present in at least 5 patients (**Supplementary Table 2**). We did not detect any recurrent NCMs in CRRs within 2kb of *KRAS*, *TP53*, *CDKN2A*, *SMAD4*, *ARID1A* and *MLL3*, in addition to 24 of 26 other PDA genes identified from previous whole exome analyses (**Supplementary Table 2**)[2,3]. This result is consistent with defects in protein function, rather than alterations in expression, in the pathogenesis of these PDA genes.

Novel clinical outcomes from pathway analysis

Pathway analysis of recurrently mutated PDA genes has been used to identify signaling networks and biological processes underlying disease pathogenesis[2,3]. To detect patterns in NCM localization at the pathway level, we utilized The Database for Annotation, Visualization and Integrated Discovery (DAVID), a functional annotation enrichment algorithm for large-scale biological datasets[35]. Pathway analysis of genes near CRRs containing clusters of mutations (>5 patients) identified significant enrichment of several gene families and regulatory processes, including transcriptional regulation, homeobox genes, axon guidance, cell adhesion and Wnt signaling (**Fig. 3c**). The involvement of three of these pathways (axon guidance, cell adhesion, Wnt signaling) in PDA has been identified from previous exome sequencing studies[2,3]. Furthermore, several homeobox genes and transcription factors have been implicated in PDA pathogenesis, including *PAX6*[36], *HOXB2*[37], *HOXB7*[38] and *RUNX3*[39]. Therefore, NCMs display preferential patterns of localization in the PDA genome and, although not found near canonical PDA genes, may act through modulation of canonical PDA pathways. In addition, we uncover a

previously unrecognized localization of NCMs near transcriptional regulators and homeobox genes, suggesting a role for these factors in PDA.

The availability of matched gene expression data from a large number (n=96) of patient samples allowed association studies between specific clusters of mutations and changes in gene expression. For each of the 124,075 CRRs we determined differential gene expression between patients with mutations in a proximal CRR compared to patients without mutations. Using permutation testing we identified NCMs that significantly impacted expression of their proximal gene and calculated their false discovery rates (for details, see **Online Methods**). Many of the genes with the greatest number of mutations (**Fig. 3a**) did not reveal significant changes in gene expression. However, this analysis yielded 16 NCMs associated with significant changes in gene expression (≥3 patients, $p<0.05$, FDR<0.25) (**Fig. 4a**). Eight of the 16 NCMs were present in regions marked by H3K4me3 and H3K27ac in PANC-1 cells. None of the statistically significant mutations were associated with increases in gene expression. Three of the genes with statistically significant decreases in expression (*KCNQ1*, *IKZF1*, *TUSC7*) have been implicated as tumor suppressors[40,41], while two (*PTPRN2*, *SNRPN*) are frequently hypermethylated[42,43]. Next, we looked for correlations between NCM-associated differential expression and clinical correlates in PDA. The small sample size precluded identification of specific NCMs associated with differences in patient outcome. Therefore, we looked for associations between expression of these 16 genes and patient outcome. Low mRNA expression of the phosphatase *PTPRN2* and the ion transporter *SLC12A8* were associated with decreased overall survival and decreased disease-free survival in a univariate analysis, respectively (**Fig. 4b,c**). Furthermore, a multivariate analysis revealed *PTPRN2* as an independent prognostic variable for overall survival (**Supplementary Table 3**).

Mechanisms of NCM-modulated expression

To uncover mechanisms by which expression-correlated SNPs may influence transcription, we annotated mutations with their predicted influence on local DNase hypersensitivity using the software Basset[44] (**see Online Methods**). The predicted influences of these 55 SNPs were significantly greater in magnitude after Bonferroni correction than a null model of sampling from the full set in 160 out of 164 examined cell types. For example, two different mutations in IRF1 and PRDM1 motifs altered critical positions that likely debilitate binding within an intron of *SLC12A8* (**Fig. 4d**). Additional mutations modulate an NRF1 motif in the promoter of *SNRPN* and a GATA motif adjacent to a PU.1 binding site in an intron of

LSAMP (**Supplementary Fig. 4**). Therefore, GECCO enriches for NCMs with predicted effects on DNase hypersensitivity and transcription factor binding.

While the Basset analysis identified NCMs predicted to affect DNase hypersensitivity, we sought to uncover NCMs directly modulating gene expression. To determine the functional relevance of specific NCMs, we performed luciferase reporter assays in non-transformed HEK-293 cells and the MiaPaCa2 and Suit2 PDA cell lines, comparing gene expression driven by wild type (WT) and mutant (MUT) sequences (**Fig. 5)**. Among 11 regions tested, 7 (293) and 4 (MiaPaCa2, Suit2) mutations significantly altered luciferase expression. Importantly, NCMs associated with *PTPRN2*, *PDPN*, *TUSC7*, *SNRNP* and *MTERF4* significantly decreased luciferase expression in one or multiple cell lines, consistent with decreased expression of these genes associated with NCMs in patient samples (**Fig. 4a**). Our validation rate was greater or comparable in terms of hit rate, and greater in terms of fold change, than other recent attempts to identify NCMs driving differential expression[15,16], highlighting the power of GECCO to identify functionally significant NCMs from millions of candidate mutations.

Mutational and expression patterns of CRR classes

The second module of GECCO focuses on CRR classes, rather than individual genes, to identify mutational patterns and overall effects on gene expression of each CRR class (**Figure 6**). We computed the mutation rate for each CRR class correcting for element size and abundance in the genome. We found no significant effect of GC content on CRR class mutation rate. Noncoding mutations were specifically enriched in certain classes of gene-proximal CRRs (see **Supplementary Note**). Next, we sought to understand the molecular characteristics of each CRR class in terms of effect on gene expression. We calculated an expression modulation score (EMS) for each CRR class reflecting the impact of the presence of that CRR on the expression of the neighboring gene in relation to all other genes. This method compared, for each CRR class, mean expression of genes proximal to a CRR to those that are non-proximal. CRRs with strong predicted activating or repressing activity would be proximal to genes with expression levels substantially higher (for activators) or substantially lower (for repressors) than the basal genome expression level (**Supplementary Table 4, see Online Methods**). To determine if the strongest activators and repressors were enriched for those CRRs with the highest mutational frequencies, we considered any activator or repressor that was greater than 1 standard deviation from the mean EMS (12 activators, 9 repressors) (**Fig. 6, green and orange bars**). The mutational frequencies for each group (activators, repressors, all others with balanced expression) were then calculated and activators and repressors compared to the

balanced group (p=0.02077 for activators vs. balanced; p=0.04982 for repressors vs. balanced). The CRR classes with the highest percentage of mutations across all PDA patients were enriched on either end of the spectrum (most repressive or most active), suggesting that recurrent NCMs are preferentially located in CRR classes with the strongest impact on gene expression. These highly active CRR classes have the largest effect on gene expression and may, therefore, confer a selective advantage to the cell. In addition, we noted that the 6 genes identified from the shRNA survival screen (**Fig. 3a**) were all associated with NCMs in highly repressive CRRs.. In contrast, every gene that failed to score in the shRNA survival screen was associated with highly active CRRs (**Fig. 3a**).

Pathway dynamics between activating and repressing CRRs

Next, we investigated the patterns of noncoding SUZ12 mutations in our patient cohort, as SUZ12 had the highest repressive score and SUZ12 sites were frequently mutated (**Supplementary Table 4, Fig. 6**). We generated two distinct lists of SUZ12-associated genes. The first list contained those genes associated with recurrently mutated SUZ12 sites. The second list contained those genes associated with SUZ12 sites that never harbored recurrent NCMs. We then performed pathway analysis on each gene set to identify differences in biological functions (**Fig. 7a**). We found that genes without recurrent SUZ12 mutations were enriched in glycoproteins, intracellular signaling as well as the axon guidance/neuron differentiation pathway. In contrast, genes with recurrent SUZ12 mutations were more significantly enriched in homeobox genes, transcription factors, Wnt signaling, proto-oncogenes and the axon guidance/neuron differentiation pathway. Surprisingly, several categories, including glycoproteins, intracellular signaling and extracellular matrix, were completely absent within the mutant SUZ12 gene set. Therefore, there is specificity for the location of NCMs in PDA, not only for certain CRRs, but also for the corresponding cancer-associated genes and pathways.

To further characterize pathways downstream of commonly mutated repressive CRRs, we performed pathway analysis on genes with and without associated CTBP2 mutations (**Fig. 7a**). Genes without CTBP2 noncoding mutations showed a similar pattern of pathway regulation as SUZ12.. These pathways were markedly enriched in the gene set associated with CTBP2 mutations, while alternative splicing and glycoproteins were completely absent. We extended this analysis to another repressive CRR with a high mutational frequency, SETDB1 (**Fig. 6a**). Genes associated with recurrent NCMs in SETDB1 binding sites were enriched in axon guidance/neuron differentiation, cell adhesion and disease mutation pathways. Therefore,

mutations in highly repressive CRRs are enriched in PDA and selectively associated with genes regulating a core set of biological processes.

We performed a similar analysis for the commonly mutated activator CRRs, including KAT2A, BCLAF1, TAF7 and WRNIP1 (**Fig. 7b**) and again found specificity for the genes and pathways that are commonly mutated. For all CRRs, there were significant differences in the pathways regulated by genes with or without mutations in a given CRR. KAT2A, BCLAF1 and TAF7 shared a very similar pattern of pathway regulation, with significant increases in nucleosome assembly/organization, methylation and ubiquitin conjugation, all processes involved in chromatin dynamics. This suggests that genes associated with NCMs in transcriptional repressors regulate homeobox genes and PDA-associated pathways, while genes associated with NCMs in transcriptional activators may regulate transcriptional dynamics through modulation of chromatin states.

DISCUSSION

We developed a new computational method, GECCO, to systematically analyze the noncoding genome of PDA to uncover recurrent regulatory somatic mutations. We find patterns of NCMs associated with genes regulating canonical PDA pathways, but not associated with commonly mutated PDA genes. Therefore, NCMs may serve as a novel mechanism in cancer cells for regulating pathways critical for tumorigenesis. Furthermore, GECCO uncovers mutations correlated with changes in gene expression, including several known tumor suppressors and aberrantly methylated genes. GECCO produces a set of high confidence calls that enrich for predicted effects on DNase hypersensitivity and transcription factor binding, as well as functional effects on gene expression, as experimentally demonstrated by luciferase reporter assays. We find enrichment for NCMs in specific CRRs and distinct subsets of pathways associated with NCMs in highly repressive and transcriptionally active CRRs as identified by our EMS algorithm. To our knowledge, this is the first comprehensive analysis of noncoding alterations in PDA, providing novel insights into PDA pathogenesis and serving as a counterpart to the information gleaned from large-scale exome sequencing projects[2,3].

Mutational analysis of patient tumors is increasingly informing treatment decisions, whereas complimentary techniques, including microarray, RNA sequencing, fluorescence *in situ* hybridization and immunohistochemistry are required to analyze changes in gene or protein expression of cancer drivers that lack coding mutations. As somatic mutations in DNA

regulatory elements can alter gene expression of cancer drivers, targeted or whole genome sequencing may provide clinically useful information for these patients, both in terms of therapeutic decisions and clinical prognosis. Our analysis provides the first collection of NCMs that correlate with changes in gene expression in PDA. Furthermore, we uncover clinical outcome relationships for *PTPRN2* and *SLC12A8*, neither of which has previously been implicated in PDA.

Functional validation of NCM-gene expression associations is a critical step in evaluating the robustness of an analysis pipeline. Our luciferase reporter assay experiments demonstrated that GECCO has a higher validation rate in cancer cell lines than any recent study of NCMs[15,16]. Furthermore, the validation rate in HEK293 cells, a standard cell line for luciferase assays, was 64%, concordant with the expected false discovery rate. Finally, GECCO accurately predicted the directionality of gene expression changes associated with NCMs. NCMs associated with *PTPRN2*, *PDPN*, *TUSC7*, *SNRNP* and *MTERF4* significantly decreased luciferase expression in one or multiple cells lines, consistent with decreased gene expression of these genes associated with NCMs in patient samples. This is in contrast to a recent report where the directionality of gene expression changes in the luciferase assay was not consistent with the predicted response[16]. Therefore, GECCO represents a significant improvement in the ability to identify functionally relevant NCMs.

Pathway analysis of the gene lists generated by GECCO revealed several unexpected findings. Strikingly, we found that the most highly recurrent somatic NCMs were located near genes in known PDA-associated pathways, including axon guidance, cell adhesion and Wnt signaling, but not the most commonly mutated PDA genes.. This suggests that NCMs may drive tumor progression through modulation of PDA-specific pathways, providing an alternative route for pathway activation and a novel mechanism of tumorigenesis. Furthermore, we provide evidence that NCMs in specific regulatory element classes are selected for during tumor evolution. These highly mutated regulatory element classes are predominantly those with the greatest impact on gene expression. Therefore, clusters of NCMs are enriched in gene-proximal regions with the greatest regulatory impact, again providing evidence for selection during tumorigenesis.

Pathway analysis of genes near NCMs within these highly mutated regulatory regions shows selectivity for PDA pathways. These pathways are not enriched when analyzing genes without associated clusters of NCMs, again arguing in favor of selection. Interestingly, many transcriptional regulators bind selectively to different regions of the genome in malignant versus non-neoplastc cells[45]. We propose that NCMs found within promoters of PDA pathway genes

modify regulatory factor binding to alter gene transcription, thereby providing an additional mechanism to promote cancer.

DATA AVAILABILITY STATEMENT

All data used in this analysis were downloaded from the International Cancer Genome Consortium (IGCG) data portal (https://dcc.icgc.org/projects). At our last date of access (Feb 11, 2015), simple somatic mutations (SSM) for 405 pancreatic ductal adenocarcinoma samples were available from the Australian (PACA-AU) and Canadian (PACA-CA) groups. We download the clinical data, SSMs, and when available, sequence-based gene expression (EXP-S) data for all 405 patients.

ACKNOWLEDGEMENTS

The authors wish to thank the members of the Tuveson lab, C. Vakoc and A. Siepel for helpful discussions. DAT is a distinguished scholar of the Lustgarten Foundation and Director of the Lustgarten Foundation-designated laboratory of Pancreatic Cancer Research. DAT is also supported by the Cold Spring Harbor Laboratory Association, the Carcinoid Foundation, PCUK, and the David Rubinstein Center for Pancreatic Cancer Research at MSKCC. In addition, we are grateful for support from the following: the STARR foundation (I7-A718 for DAT), DOD (W81XWH-13-PRCRP-IA for DAT), Louis Morin Charitable Trust (MEF) and the NIH (5P30CA45508-26, 5P50CA101955-07, 1U10CA180944-01, 5U01CA168409-3, and 1R01CA190092-01 for DAT and R01HG006677 for MCS).

AUTHOR CONTRIBUTIONS

Wrote the manuscript: MEF, TG, MCS, DAT

Supervised the study: MCS, DAT

Performed FunSeq analysis and developed GECCO: TG

Performed pathway analysis: MEF

Contributed to data analysis: MEF, TG, SMG, AVB, EK, SS, LDS, SG, JDM

Performed patient outcome analysis: DC, PB

Performed Basset analysis: DRK

Performed germline sequence analysis: NW

COMPETING FINANCIAL INTERESTS STATEMENT

The authors declare no competing financial interests.

REFERENCES

1. Siegel, R., Naishadham, D. & Jemal, A. Cancer statistics, 2013. *CA: a cancer journal for clinicians* **63**, 11-30 (2013).
2. Jones, S.*, et al.* Core signaling pathways in human pancreatic cancers revealed by global genomic analyses. *Science* **321**, 1801-1806 (2008).
3. Biankin, A.V.*, et al.* Pancreatic cancer genomes reveal aberrations in axon guidance pathway genes. *Nature* **491**, 399-405 (2012).
4. Waddell, N.*, et al.* Whole genomes redefine the mutational landscape of pancreatic cancer. *Nature* **518**, 495-501 (2015).
5. Huang, F.W.*, et al.* Highly recurrent TERT promoter mutations in human melanoma. *Science* **339**, 957-959 (2013).
6. Horn, S.*, et al.* TERT promoter mutations in familial and sporadic melanoma. *Science* **339**, 959-961 (2013).
7. Bell, R.J.*, et al.* The transcription factor GABP selectively binds and activates the mutant TERT promoter in cancer. *Science* (2015).
8. Killela, P.J.*, et al.* TERT promoter mutations occur frequently in gliomas and a subset of tumors derived from cells with low rates of self-renewal. *Proc Natl Acad Sci U S A* **110**, 6021-6026 (2013).
9. Rachakonda, P.S.*, et al.* TERT promoter mutations in bladder cancer affect patient survival and disease recurrence through modification by a common polymorphism. *Proc Natl Acad Sci U S A* **110**, 17426-17431 (2013).
10. Mansour, M.R.*, et al.* An oncogenic super-enhancer formed through somatic mutation of a noncoding intergenic element. *Science* **346**, 1373-1377 (2014).
11. Weinhold, N., Jacobsen, A., Schultz, N., Sander, C. & Lee, W. Genome-wide analysis of noncoding regulatory mutations in cancer. *Nat Genet* **46**, 1160-1165 (2014).
12. Fredriksson, N.J., Ny, L., Nilsson, J.A. & Larsson, E. Systematic analysis of noncoding somatic mutations and gene expression alterations across 14 tumor types. *Nat Genet* **46**, 1258-1263 (2014).
13. Melton, C., Reuter, J.A., Spacek, D.V. & Snyder, M. Recurrent somatic mutations in regulatory regions of human cancer genomes. *Nat Genet* (2015).
14. Mathelier, A.*, et al.* Cis-regulatory somatic mutations and gene-expression alteration in B-cell lymphomas. *Genome biology* **16**, 84 (2015).
15. Araya, C.L.*, et al.* Identification of significantly mutated regions across cancer types highlights a rich landscape of functional molecular alterations. *Nat Genet* **48**, 117-125 (2016).
16. Fujimoto, A.*, et al.* Whole-genome mutational landscape and characterization of noncoding and structural mutations in liver cancer. *Nat Genet* **48**, 500-509 (2016).
17. International Cancer Genome, C.*, et al.* International network of cancer genome projects. *Nature* **464**, 993-998 (2010).
18. Khurana, E.*, et al.* Integrative annotation of variants from 1092 humans: application to cancer genomics. *Science* **342**, 1235587 (2013).
19. Fu, Y.*, et al.* FunSeq2: A framework for prioritizing noncoding regulatory variants in cancer. *Genome biology* **15**, 480 (2014).
20. Consortium, E.P. An integrated encyclopedia of DNA elements in the human genome. *Nature* **489**, 57-74 (2012).

21. Teng, Y., Mei, Y., Hawthorn, L. & Cowell, J.K. WASF3 regulates miR-200 inactivation by ZEB1 through suppression of KISS1 leading to increased invasiveness in breast cancer cells. *Oncogene* **33**, 203-211 (2014).
22. Winham, S.J.*, et al.* Genome-wide investigation of regional blood-based DNA methylation adjusted for complete blood counts implicates BNC2 in ovarian cancer. *Genetic epidemiology* **38**, 457-466 (2014).
23. Dulak, A.M.*, et al.* Exome and whole-genome sequencing of esophageal adenocarcinoma identifies recurrent driver events and mutational complexity. *Nat Genet* **45**, 478-486 (2013).
24. Sherman, S.K.*, et al.* Gastric inhibitory polypeptide receptor (GIPR) is a promising target for imaging and therapy in neuroendocrine tumors. *Surgery* **154**, 1206-1213; discussion 1214 (2013).
25. Uzawa, K.*, et al.* Targeting phosphodiesterase 3B enhances cisplatin sensitivity in human cancer cells. *Cancer medicine* **2**, 40-49 (2013).
26. Renjie, W. & Haiqian, L. MiR-132, miR-15a and miR-16 synergistically inhibit pituitary tumor cell proliferation, invasion and migration by targeting Sox5. *Cancer letters* **356**, 568-578 (2015).
27. Sandelin, A., Alkema, W., Engstrom, P., Wasserman, W.W. & Lenhard, B. JASPAR: an open-access database for eukaryotic transcription factor binding profiles. *Nucleic acids research* **32**, D91-94 (2004).
28. Flandin, P.*, et al.* Lhx6 and Lhx8 coordinately induce neuronal expression of Shh that controls the generation of interneuron progenitors. *Neuron* **70**, 939-950 (2011).
29. Boon, M.R.*, et al.* Bone morphogenetic protein 7: a broad-spectrum growth factor with multiple target therapeutic potency. *Cytokine & growth factor reviews* **22**, 221-229 (2011).
30. Gutschner, T.*, et al.* The noncoding RNA MALAT1 is a critical regulator of the metastasis phenotype of lung cancer cells. *Cancer Res* **73**, 1180-1189 (2013).
31. Moriyama, T.*, et al.* MicroRNA-21 modulates biological functions of pancreatic cancer cells including their proliferation, invasion, and chemoresistance. *Molecular cancer therapeutics* **8**, 1067-1074 (2009).
32. Cheung, H.W.*, et al.* Systematic investigation of genetic vulnerabilities across cancer cell lines reveals lineage-specific dependencies in ovarian cancer. *Proc Natl Acad Sci U S A* **108**, 12372-12377 (2011).
33. Lan, Q.*, et al.* Genetic susceptibility for chronic lymphocytic leukemia among Chinese in Hong Kong. *European journal of haematology* **85**, 492-495 (2010).
34. Sun, H.T., Cheng, S.X., Tu, Y., Li, X.H. & Zhang, S. FoxQ1 promotes glioma cells proliferation and migration by regulating NRXN3 expression. *PLoS One* **8**, e55693 (2013).
35. Huang da, W., Sherman, B.T. & Lempicki, R.A. Systematic and integrative analysis of large gene lists using DAVID bioinformatics resources. *Nature protocols* **4**, 44-57 (2009).
36. Mascarenhas, J.B.*, et al.* PAX6 is expressed in pancreatic cancer and actively participates in cancer progression through activation of the MET tyrosine kinase receptor gene. *J Biol Chem* **284**, 27524-27532 (2009).

37. Segara, D., *et al.* Expression of HOXB2, a retinoic acid signaling target in pancreatic cancer and pancreatic intraepithelial neoplasia. *Clinical cancer research : an official journal of the American Association for Cancer Research* **11**, 3587-3596 (2005).
38. Chile, T., *et al.* HOXB7 mRNA is overexpressed in pancreatic ductal adenocarcinomas and its knockdown induces cell cycle arrest and apoptosis. *BMC cancer* **13**, 451 (2013).
39. Whittle, M.C., *et al.* RUNX3 Controls a Metastatic Switch in Pancreatic Ductal Adenocarcinoma. *Cell* **161**, 1345-1360 (2015).
40. Than, B.L., *et al.* The role of KCNQ1 in mouse and human gastrointestinal cancers. *Oncogene* **33**, 3861-3868 (2014).
41. Geimer Le Lay, A.S., *et al.* The tumor suppressor Ikaros shapes the repertoire of notch target genes in T cells. *Science signaling* **7**, ra28 (2014).
42. Anglim, P.P., *et al.* Identification of a panel of sensitive and specific DNA methylation markers for squamous cell lung cancer. *Molecular cancer* **7**, 62 (2008).
43. Benetatos, L., *et al.* CpG methylation analysis of the MEG3 and SNRPN imprinted genes in acute myeloid leukemia and myelodysplastic syndromes. *Leukemia research* **34**, 148-153 (2010).
44. Kelley, D.R., Snoek, J. & Rinn, J.L. Basset: learning the regulatory code of the accessible genome with deep convolutional neural networks. *Genome research* **26**, 990-999 (2016).
45. Squazzo, S.L., *et al.* Suz12 binds to silenced regions of the genome in a cell-type-specific manner. *Genome research* **16**, 890-900 (2006).
46. Weirauch, M.T., *et al.* Determination and inference of eukaryotic transcription factor sequence specificity. *Cell* **158**, 1431-1443 (2014).
47. Gupta, S., Stamatoyannopoulos, J.A., Bailey, T.L. & Noble, W.S. Quantifying similarity between motifs. *Genome biology* **8**, R24 (2007).

FIGURE LEGENDS

Figure 1 - Identification of recurrent noncoding mutations in PDA.

(a) The total number of single nucleotide variants (SNV) was plotted for each patient. **(b)** FunSeq2 was utilized to detect and characterize putatitve somatic noncoding mutations from 308 PDA whole genome sequences. Mutation counts for each functional category are displayed. **(c)** The number of *cis*-regulatory region (CRR) mutations (grey bars), and CRR/total SNV (black points) were plotted for each patient.

Figure 2 - GECCO (Genomic Enrichment Computational Clustering Operation) flowchart.

GECCO utilizes noncoding somatic mutation calls from tumor whole genome sequencing data to identify clusters of mutations within 2kb of genes, including those that correlate with changes in gene expression. GECCO also calculates the mutation rate of gene regulatory regions and determines the strength of each regulatory region in terms of the effect on gene expression (expression modulation score, EMS). These data can then be used for pathway analysis of genes proximal to noncoding clusters and genes downstream of specific regulatory regions. The gene lists can also be interrogated for patient survival analysis when coupled to outcome data for detection of clinically relevant interactions.

Figure 3 - Clustered gene-proximal mutations and pathways in PDA.

(a) The most common mutational clusters across the patient cohort as determined by GECCO, with associated genes; Yes = knockdown promoted cell death in shRNA cancer cell line screen. (P denotes PDA-specific); No = no evidence for effect on cell death in shRNA cancer cell line screen. **(b)** Most significant clusters when corrected for cluster size as determined by GECCO. **(c)** DAVID pathway analysis was used to identify regulatory processes and pathways from genes associated with recurrent NCMs.

Figure 4 - Recurrent gene-proximal mutations correlate with gene expression changes in PDA.

(a) GECCO used gene expression data from matched PDA patients to correlate NCMs with changes in gene expression “Mut allele” = mean expression of linked gene in patients with associated CRR mutations. “WT allele” = mean expression of linked gene in patients without associated CRR mutations. **(b)** Analysis of overall survival (OS) in PDA patients expressing high

(upper 2/3) and low (lower 1/3) levels of *PTPRN2*. Purple dots represent patients with high expression of *PTPRN2* "at risk" (alive). Red dots represent patients with low expression of *PTPRN2* "at risk" (alive). **(c)** Analysis of disease-free survival (DFS) in PDA patients expressing high (upper 2/3) and low (lower 1/3) levels of *SLC12A8*. **(d)** Two A→C mutations in a regulatory site on chromosome 3 at positions 124,840,671 and 124,840,678 alter critical nucleotides in an IRF1 and/or PRDM1 binding site. The regulatory site lies in an intron of one isoform and promoter of an alternative isoform of *SLC12A8*. At the bottom, heat map displays predicted change in accessibility, considered here as DNase-seq signal in GM12865. The line plots above measure the maximum (gain) and minimum (loss) predicted change; the loss highlights nucleotides that significantly alter the overall signal upon mutation as both of these mutations do.

Figure 5 - Noncoding mutations modulate luciferase gene expression.

(a-c) Luciferase reporter assays of WT (black) and MUT sequences (white bars) are shown for selected NCMs associated with named genes. For each box-and-whisker plot, center line is the mean, box limits are min/max values, whiskers are s.d. Data from a representative experiment (n=3 replicates) with a total of n=4 independent transfected cultures for each cell line are shown. *P* values calculated by two-tailed unpaired *t* test. (*, $p<0.05$; **, $p<0.01$; ***, $p<0.001$)

Figure 6 - Gene-proximal NCMs are enriched in specific classes of CRRs.

Percentage of CRRs with at least 2 mutations across the patient cohort, corrected for genome abundance and size, ordered from left to right by expression modulation score (EMS) (most repressive to most active). Dotted line represents mean mutation frequency across all CRRs.

Figure 7 - Gene-proximal NCMs in repressors and activators cluster near distinct subsets of genes.

(a) Pathway analysis of genes associated with recurrently mutated repressive (SUZ12, CTBP2, SETDB1) sites (red bars), versus those never harboring NCMs in those CRRs (blue bars). **(b)** Pathway analysis of genes associated with recurrently mutated activator (KAT2A, BCLAF1, TAF7, WRNIP1) sites (red bars), versus those never harboring NCMs in those CRRs (blue bars). AG/ND, axon guidance/neuron differentiation.

Supplementary Figure 1 - Identification of recurrent noncoding mutations in PDA.

Distribution of SNV rates across the patient cohort.

Supplementary Figure 2 - Overlap of SNVs and common coding mutations in PDA.
Distribution of SNVs across the patient cohort, with common coding mutations (colored bars) in PDA genes.

Supplementary Figure 3 - Overlap of gene-proximal NCMs in CRRs and common coding mutations in PDA.
Distribution of CRR mutation rates across the patient cohort, with common coding mutations (colored bars) in PDA genes.

Supplementary Figure 4 - NCMs disrupt transcription factor binding motifs.
(a) A G→A mutation in a regulatory site on chromosome 15 at position 25,200,056 alters a critical nucleotide in an NRF1 binding site. The regulatory site lies in the promoter of *SNRPN*. At the bottom, the heat map displays the predicted change in binding, considered here as ChIP-seq signal for NRF1 in H1-hESCs. The line plots above measure the maximum (gain) and minimum (loss) predicted change; the loss highlights nucleotides that significantly alter the overall signal upon mutation as this mutation does. **(b)** A G->T mutation in a regulatory site on chromosome 3 at position 115,757,580 introduces a GATA factor binding site nearby an established PU.1 binding site. The heat map displays the predicted change in accessibility, considered here as DNase-seq signal in K562. In other cells, such as monocytes, the model predicts reduced accessibility, suggesting that GATA binding here may alter the combinatorial logic of the regulatory element in a complex fashion.

Supplementary Table 1 - Genome-wide exactly recurrent mutations in PDA.
The most common exactly recurrent mutations across the patient cohort. Sequence of mutant allele in parenthesis.

Supplementary Table 2 - Distribution of gene-proximal NCMs near known PDA genes.
Analysis of the association of NCM clusters as determined by GECCO with known PDA genes.

Supplementary Table 3 - *PTPRN2* multivariate analysis.
Multivariate analysis of clinico-pathological variables and *PTPRN2* expression in the patient cohort.

Supplementary Table 4 - CRR expression modulation scores.

Effect of CRR on activity of neighboring gene compared with all other genes in the genome (see **Online Methods** for analysis details). EM Score, expression modulation score.

ONLINE METHODS

1. Data Acquisition

All data used in this analysis were downloaded from the International Cancer Genome Consortium (IGCG) data portal (https://dcc.icgc.org/projects). At our last date of access (Feb 11, 2015), simple somatic mutations (SSM) for 405 pancreatic ductal adenocarcinoma samples were available from the Australian (PACA-AU) and Canadian (PACA-CA) groups. We download the clinical data, SSMs, and when available, sequence-based gene expression (EXP-S) data for all 405 patients.

2. Pre-processing

The whole genome sequencing (WGS) required to call SNVs across all 405 patients and the whole genome RNA-sequencing required to calculate gene expression were carried out by two distinct consortiums, one Canadian and one Australian. All SNV calls (SSMs) and gene expression calculations (EXP-S) by these two groups were consolidated by ICGC.

2.1. SNV calls from whole genome sequencing

For each of the 405 patients we extracted the chromosome, start location, end location, somatic allele, and mutated allele from the list of simple somatic mutations (file: ssm_open.tsv) and converted to bed format. Many of the SNVs were redundant within patients. For each patient, the list of SNVs were sorted by genomic coordinates and consolidated to contain only a single entry for each unique SNV. A subset of patients had extremely low numbers of SNVs (likely due to poor sequencing results) or high numbers of SNVs (likely due to hyper-mutated regions, unlocalized replication defects, or microsatellite instability). Across all 405 patients the number of unique SNVs ranged from 1 to 440,471 with a mean 7,937 and a standard deviation of 26,224. In order to remove outliers we eliminated all patients with less than 100 SNVs (92 patients in total) or an SNV count more than 3 standard deviations away from the mean (5 patients in total). This left 308 patients with a mean SNV count of 7,300 and ranging from 1,040 to 68,885.

2.2. Gene expression (FPKM) from whole genome RNA-sequencing

Of the 308 patients that passed the previous filtering step, 96 had expression data available from ICGC. For each of the 96 patients, we extracted the normalized read count (FPKM) and Ensembl gene id (file: exp_seq.tsv). While the vast majority of genes have expression data

across all 96 patients, there were several thousand Ensembl genes that only contained expression data for a subset of patients. In order to streamline and simplify downstream analysis we kept only the 50,861 Ensembl genes that were shared by all 96 patients. In addition, there were three patients (DO33168, DO35098, DO35100) that had gene expression from either 2 or 3 independently sequenced samples. For these three patients, the gene expression for each gene was calculated by taking the mean across all samples.

3. Analyzing noncoding variants with GECCO

In order to identify potential noncoding cancer drivers, we first used FunSeq2 (v2.1.0) as a high level filter to prioritize our SNVs. The unique SNVs for each of the 308 patients were converted to bed format and analyzed by FunSeq2 using the command *./run.sh –inf bed –n* to identify only noncoding variants. This analysis pipeline requires a suite of annotation data that is used to make calls and score noncoding variants. These were downloaded from (http://funseq2.gersteinlab.org/data/). One of these files, "ENCODE.annotation.gz" contains the full list of TFPs/CRRs used in our analysis along with their exact genomic coordinates.

3.1 Processing recurrently mutated cis-regulatory regions (CRRs)

FunSeq2 generates a number of output files including Recur.Summary, which contains a list of all noncoding elements, the genomic coordinates of these elements, the fraction of patients with a mutation in this element, and the full list of patient names along with the genomic locations of each mutation. While the ENCODE annotation data provides a number of different noncoding elements (enhancers, transcription factor binding sites (TFPs), DNase hypersensitivity, etc.) we chose to focus our analysis on TFPs – referred to in this manuscript as CRRs – as they were the most highly represented class of elements identified. CRR proximal genes were found by intersecting CRRs with genes that had been expanded by 2kb at their 5' and 3' ends.

3.2 Calculating CRR mutation rates

As described above, the full list of CRRs (121 distinct CRR classes in total) including their counts and genomic positions can be found in "ENCODE.annotation.gz." GECCO makes two separate calculations across all 121 CRR classes using the CRR genomic information: (1) For a given CRR class, it calculates the fraction of distinct CRR sites that are mutated within the class and (2) the base level mutation rate for each CRR class (the number of mutations in all CRRs of a given class divided by the total number of base pairs of all CRRs in a given class). For an individual CRR, there are three ways in which GECCO calculates the mutational frequency: (1)

by summing the number of mutations in a given CRR, (2) by calculating the fraction of bases in the CRR that are mutated (i.e. mutation counts normalized by read length), or (3) by calculating the fraction of bases in a CRR mutation cluster. Option (3) is computed by first determining the cluster size within a CRR, the number of bases required to span all mutations in a given CRR. For example, consider a 2kb CRR with 9 mutations. If the two most distantly separated of the 9 mutations are 100bps apart then the length of the mutation cluster is 100bp. The mutational frequency of the cluster is then computed by dividing the number of mutations in that cluster by the size of the cluster (9/100 = 9.0%). This approach weights exactly recurrent or proximal mutations more strongly than distant mutations.

4. Pathway analysis

The Database for Annotation, Visualization and Integrated Discovery (DAVID), a functional annotation enrichment algorithm for large-scale biological datasets was used for pathway analysis, with the following annotation categories: SP_PIR_KEYWORDS, GOTERM_BP_FAT, KEGG_PATHWAY, PANTHER_PATHWAY, SMART. A Bonferroni corrected p-value of 0.05 was used as a cutoff for enrichment significance.

5. Survival analysis

Median survival was estimated using the Kaplan-Meier method and the difference was tested using the log-rank Test. *P* values of less than 0.05 were considered statistically significant. Clinico-pathologic variables analyzed with a *P* value of less than 0.25 on log-rank test were entered into Cox Proportional Hazard multivariate analysis, and redundant variables were eliminated using a backward elimination method. Statistical analysis was performed using StatView 5.0 Software (Abacus Systems, Berkeley, CA, USA). Overall survival (OS) or disease-free survival (DFS) was used as the primary endpoint.

PTPRN2 Expression level > 4.98 defined as high

SLC12A8 Expression level > 7.03 defined as high

6. Computing differential expression

Differential expression was computed for each recurrently mutated CRR that was within 2kb of an Ensemble gene using permutation testing. For each CRR/gene pair, the 96 patients with mutation data were split into two groups – patients with mutations in the CRR and patients without mutations in the CRR. Using the expression data downloaded from ICGC for the gene of interest a t-test is performed to generate a single t-value, the *observed t-value*. The

761 expression values for patients with mutations in CRRs and the expression values for patients
762 without mutations are then permuted 100,000 times to generate 100,000 additional t-values, the
763 permuted t-values. These t-values generally fit a Gaussian distribution to which the observed t-
764 value is then compared to using a two-tailed test. The empirical p-value is computed as the
765 fraction of times (x/100,000) that a "permuted t-value" falls further outside the Gaussian
766 distribution than the "observed t-value". Once p-values have been calculated for all recurrently
767 mutated genes proximal to CRRs, GECCO estimate q-values (the false discovery rate) for each
768 call. This is done using the "qvalue" package in R and measures the proportion of false
769 positives incurred given the p-value distribution.
770
771 **7. Luciferase Reporter Assay and Statistics**
772 150 base pair sequences surrounding specific NCMs (wild type, WT or mutant, MUT) were
773 synthesized (Integrated DNA Technologies) and cloned into pGL4.23 (Promega), containing a
774 minimal promoter driving firefly luciferase. Five thousand cells per well (HEK-293, MiaPaCa2 or
775 Suit2) were co-transfected in 96-well format with the specific WT or MUT vector and pRL-
776 SV40P (*Renilla* luciferase, Addgene #27163) as a normalization control. Luciferase activity was
777 measured 48 hours post-transfection with the Dual-Luciferase Reporter Assay System
778 (Promega). Values reported are firefly luciferase divided by *Renilla* luciferase. Analytical
779 statistics were generated in Prism 7.0 (GraphPad), and *P* values are from two-tailed unpaired *t*
780 tests. All cell lines were obtained from ATCC and tested for mycoplasma contamination.
781
782 **8. Computing Expression Modulation Scores (EMS)**
783 Some CRRs bind transcription factors or transcription factor components with well-known
784 expression modulation including SUZ12 and CTBP2, which act as transcriptional repressors, or
785 BDP1 and BRF1, which act as transcriptional activators. However, many of the 121 CRRs used
786 in this study have unexplored or unvalidated directions of expression modulation. We
787 developed a method to infer the direction and effect of expression modulation for each CRR
788 class by comparing the expression of genes proximal CRRs in a given CRR class to the mean
789 expression of all other active genes in the genome.
790
791 Many genes are inactive in any given tissue and in a given RNA-seq experiment ~50% of genes
792 show low to no expression. For all 96 patients with expression data, we found this also to be
793 true with ~50% of genes showing 0 expression. When computing the expression modulation for
794 each CRR class we ignored all genes that showed 0 expression in at least 90% of patients (86

patients or more). For a given CRR class and for each of the 96 patients we compute (1) the mean expression of all genes proximal to CRRs in that class and (2) the mean expression of all genes non-proximal to a CRR in that class. For a given CRR class we then compute the log of the ratio between (1) and (2) for each of the 96 patients and then take the mean of the log ratio for all 96 patients to get a single "expression modulation score" for each CRR class. The log of the ratio will be negative if the mean expression of genes proximal to a CRR class is lower than the genome average (repression) and will be positive if the mean expression of genes proximal to a CRR class is higher than the genome average (activation). This calculation is *not meant* to generate absolute numerical score for the repressive or activating activity of a CRR but is instead used to generate a *rank-sorted* list of CRR classes based on their expression modulation.

9. Basset Analysis

Basset is a recently introduced method based on convolutional neural networks to accurately predict DHSs from DNA sequence, thus enabling annotation of the influence of mutations on accessibility[44]. We trained the Basset deep convolutional neural network on DHSs from 164 cell types mapped by ENCODE and the Roadmap Epigenomics projects. From this, we predicted the influence of variants on the presence of DNase hypersensitivity in each cell type by computing the difference between predictions on sequences with each allele. Candidate high impact variants were further analyzed for interrupting known binding sites by converted Basset-learned first convolution layer filters to probabilistic position weight matrixes by counting nucleotide occurrences in the set of sequences that activate the filter to a value that is more than half of its maximum value. We identified the likely binding protein for the motifs by querying the CIS-BP database[46] (accessed on June 12, 2015) using the TomTom v4.10.1 search tool[47] and requiring an FDR q-value < 0.1.

*All code can be requested by e-mailing MCS.

a

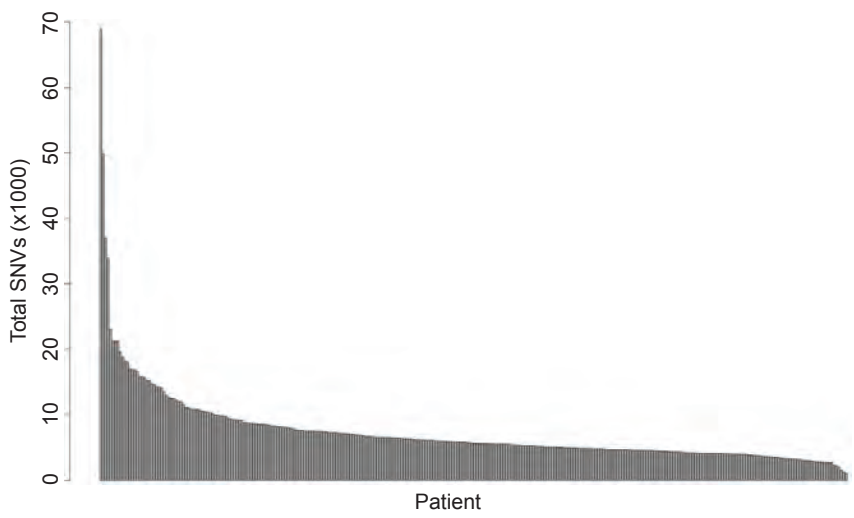

b **FunSeq variants in pancreatic ductal adenocarcinoma (n=308)**

Variant class	Total
Transcription factor binding peak/*cis*-regulatory region (CRR)	264,488
Enhancer	19,608
DNaseI hypersensitive site	14,572
Pseudogene	1,632
lincRNA	1,104
Transcription factor motif within peak	135
Miscellaneous RNA	24
miRNA	19
snRNA	6
snoRNA	4
rRNA	4

c

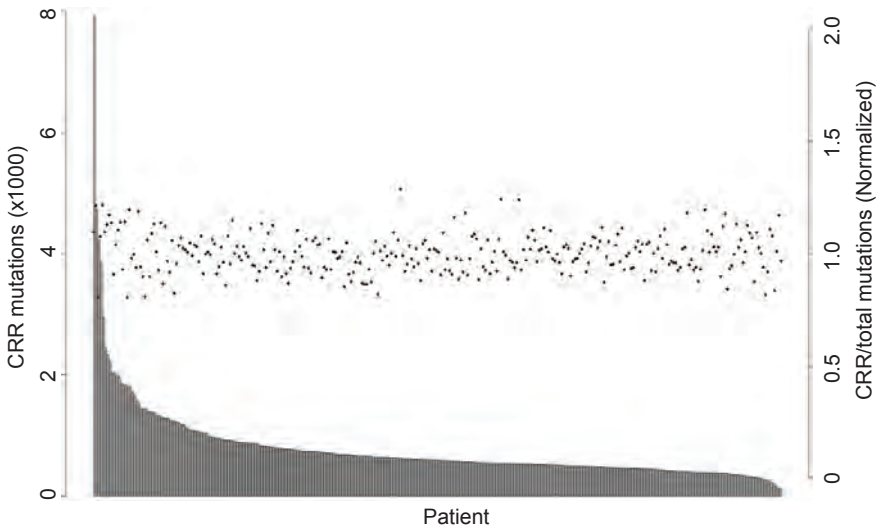

Figure 1 - Identification of recurrent noncoding mutations in PDA.
(a) The total number of single nucleotide variants (SNV) was plotted for each patient. **(b)** FunSeq2 was utilized to detect and characterize putatitve somatic noncoding mutations from 308 PDA whole genome sequences. Mutation counts for each functional category are displayed. **(c)** The number of *cis*-regulatory region (CRR) mutations (grey bars), and CRR/total SNV (black points) were plotted for each patient.

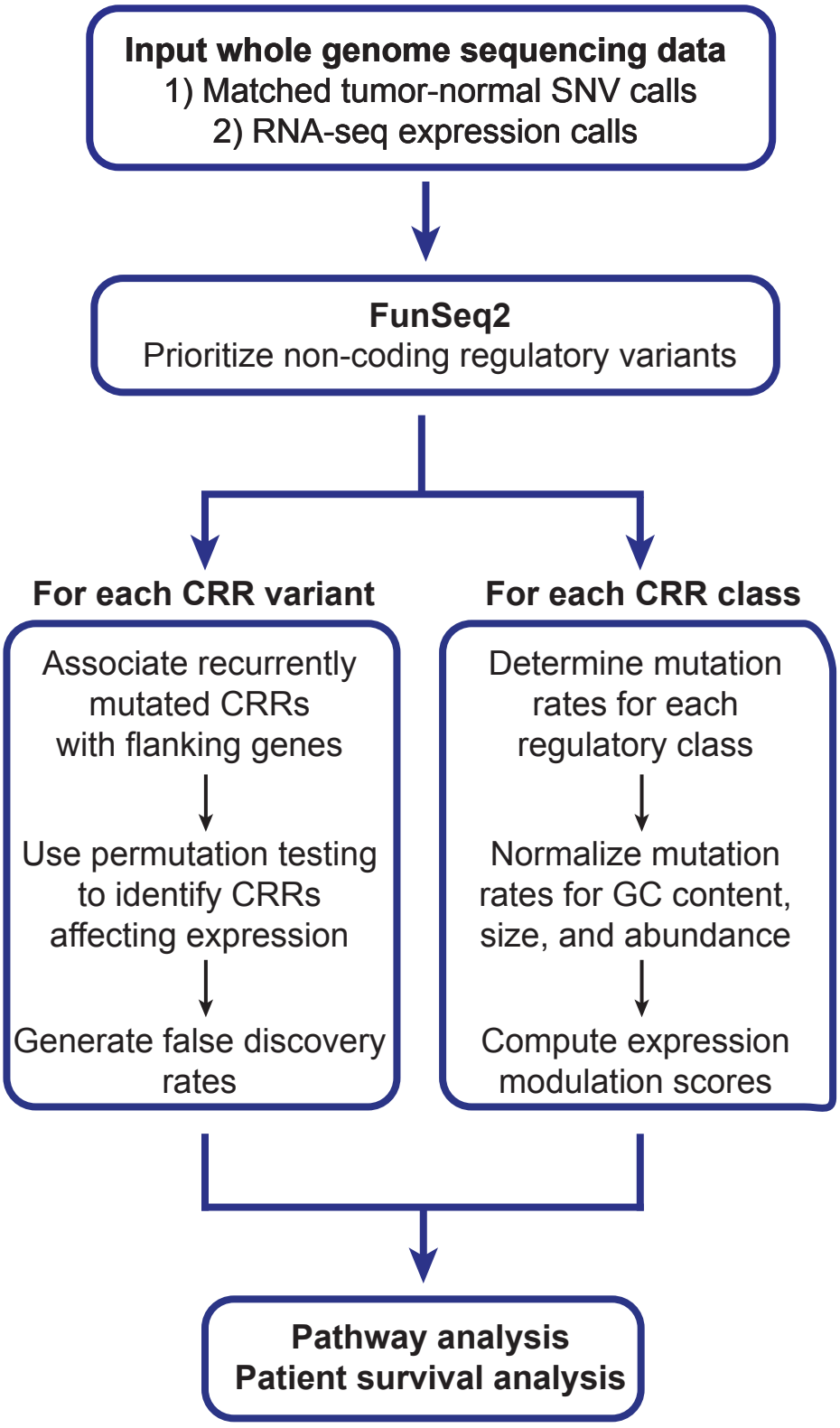

Figure 2 - GECCO (Genomic Enrichment Computational Clustering Operation) flowchart.
GECCO utilizes noncoding somatic mutation calls from tumor whole genome sequencing data to identify clusters of mutations within 2kb of genes, including those that correlate with changes in gene expression. GECCO also calculates the mutation rate of gene regulatory regions and determines the strength of each regulatory region in terms of the effect on gene expression (expression modulation score, EMS). These data can then be used for pathway analysis of genes flanking noncoding clusters and genes downstream of specific regulatory regions. The gene lists can also be interrogated for patient survival analysis when coupled to outcome data for detection of clinically relevant interactions.

a Noncoding gene-proximal mutational clusters in PDA

CRR	Nearest gene	Patients (%)	Gene name/protein function	shRNA
TCF12	*LHX8*	17 (5.52%)	LIM homeobox 8	Yes
JUND	LINC01194	16 (5.19%)	long intergenic non-protein coding RNA	NA
E2F1	*BMP7*	15 (4.87%)	bone morphogenetic protein 7	No
SUZ12	*LHX8*	15 (4.87%)	LIM homeobox 8	
WRNIP1	*DUSP22*	15 (4.87%)	dual specificity phosphatase 22	No
EP300	REREP3	14 (4.55%)	arginine-glutamic acid dipeptide (RE) repeats pseudogene 3	NA
SUZ12	*LMX1B*	14 (4.55%)	LIM homeobox txn factor	Yes (P)
SUZ12	*PAX6*	14 (4.55%)	paired box 6, homeodomain	Yes
TCF12	*ZIC4*	14 (4.55%)	zinc-finger family member 4	No
HDAC2	*FANK1*	14 (4.55%)	fibronectin type 3 and ankyrin repeat domains 1	No
FOXA1	REREP3	13 (4.22%)	arginine-glutamic acid dipeptide (RE) repeats pseudogene 3	NA
NFKB1, POU2F2	*ST8SIA4*	13 (4.22%)	ST8 alpha-N-acetyl-neuraminide alpha-2,8-sialyltransferase 4	No
SIN3A	MIR21	13 (4.22%)	microRNA21	NA
SIN3A	*VMP1*	13 (4.22%)	vacuole membrane protein 1	No
SUZ12	*DMRTA2*	13 (4.22%)	doublesex-and Mab-3-related transcription factor A2	Yes
SUZ12	*VAX2*	13 (4.22%)	ventral anterior homeobox 2	Yes
SUZ12	*ZIC4*	13 (4.22%)	zinc-finger family member 4	
BCLAF1	*DUSP22*	12 (3.90%)	dual specificity phosphatase 22	
BCLAF1	MALAT1	12 (3.90%)	Metastasis Associated Lung Adenocarcinoma Transcript 1 (lncRNA)	NA
BCLAF1	*VMP1*	12 (3.90%)	vacuole membrane protein 1	
CDH2, JUND	*ZNF595*	12 (3.90%)	zinc-finger txn factor	No
CDH2, JUND	*ZNF718*	12 (3.90%)	zinc-finger txn factor	No
FOXA1	*CDH15*	12 (3.90%)	cadherin 15, type 1, M-cadherin	Yes (P)
HDAC2	*CDH8*	12 (3.90%)	cadherin 8, type 2	No

b Corrected for bounded gene-proximal CRR

CRR	Nearest gene	Patients (%)	Cluster (bp)	Mutation freq. (%)	Gene name/protein function
BHLHE40	*ACOXL*	5 (1.62%)	1	>100	acyl-CoA oxidase-like
RAD21	*NRXN3*	5 (1.62%)	19	26.32	neurexin 3, neuronal cell adhesion
MAFK	*MACROD2*	5 (1.62%)	55	9.09	O-acetyl-ADP-ribose deacetylase
EGR1	*ARSD*	5 (1.62%)	65	7.69	arylsulfatase D
REST	*LILRA5*	5 (1.62%)	81	6.17	leukocyte immunoglobulin-like receptor
CEBPB	*PDE4B*	6 (1.95%)	129	4.65	phosphodiesterase 4B, cAMP-specific
NRF1	*ANXA11*	5 (1.62%)	134	3.73	annexin A11
GATA2	*XKR6*	5 (1.62%)	145	3.45	Kell blood group complex-related
NR3C1	*PXDN*	7 (2.27%)	223	3.14	phroxidasin Homolog
JUND	*NBPF25P*	5 (1.62%)	162	3.09	neuroblastoma breakpoint family, pseudogene
STAT3	*SORCS1*	6 (1.95%)	205	2.93	sortilin-related VPS10 domain containing receptor
USF1	*SCAI*	5 (1.62%)	171	2.92	suppressor of cancer cell invasion
BRF2	FRG1B	5 (1.62%)	186	2.69	FSHD region gene 1 family, lncRNA
CEBPB	*NRXN1*	5 (1.62%)	227	2.20	neurexin 1, neuronal cell adhesion
ZNF263	LINC00693	6 (1.95%)	283	2.12	uncharacterized lncRNA

c Pathways regulated by NCMs in pancreatic ductal adenocarcinoma

Regulatory process/gene family	# genes altered	*p*-value	Representative altered genes
Regulation of transcription	135	3.9E-15	*ALX4, DMRTA2, T, TWIST1, RUNX3, WWTR1*
Homeobox	45	6.2E-26	*LHX5, NKX2-8, HOXB4, IRX1, MSX1, VAX2*
Neuron differentiation/axon guidance	53	1.1E-19	*ROBO1, SLIT2, NRXN1, CTNNA2, NCAM2, BDNF*
Cell adhesion	24	2.8E-4	*CDH15, CDH8, CADM1, ITGB2, LAMA5, CNTN4*
Wnt signaling pathway	18	4.3E-2	*FZD10, FBXW11, NKD1, TCF7L1, EN2*

Figure 3 - Clustered gene-proximal mutations and pathways in PDA.
(a) The most common mutational clusters across the patient cohort as determined by GECCO, with associated genes; Yes = knockdown promoted cell death in shRNA cancer cell line screen. (P denotes PDA-specific); No = no evidence for effect on cell death in shRNA cancer cell line screen; CRR=FunSeq2-defined *cis*-regulatory region. **(b)** Most significant clusters when corrected for cluster size as determined by GECCO. **(c)** DAVID pathway analysis was used to identify regulatory processes and pathways from genes associated with recurrent NCMs.

a **NCMs correlate with gene expression changes**

CRR (MUT#)	Nearest gene	MUT allele	WT allele	Fold change	*p*-value	q-value
MAX (5)	*PTPRN2*	0.82	10.92	0.075	0.00593	0.09689
FOSL2 (7)	*KCNQ1*	0.85	6.39	0.133	0.02456	0.18212
TAF7 (9)	*SNRPN*	0.46	3.4	0.135	0.00818	0.11818
NFKB1 (7)	*GYPC*	1.08	7.29	0.148	0.01845	0.15157
TAF1 (6)	*PDPN*	2.09	13.08	0.160	0.03544	0.22016
BCLAF1 (5)	*PRSS12*	1.07	6.46	0.166	0.01107	0.14144
MAFK (3)	*SOX5*	0.29	1.63	0.178	0.02851	0.20379
POU2F2 (6)	MIR4420	8.16	40.24	0.203	0.01773	0.15157
WRNIP1 (3)	*IKZF1*	0.64	3.15	0.203	0.01811	0.15157
GATA3 (3)	*PCLO*	0.35	1.67	0.210	0.01113	0.14144
JUND (3)	TUSC7	0.98	4.53	0.216	0.02909	0.20560
REST (3)	*MTERF4*	1.46	5.78	0.253	0.02209	0.16542
GATA1 (3)	*FNIP2*	7.59	18.32	0.414	0.02588	0.18929
CEBPB (3)	*PNPLA8*	5.69	13.62	0.418	0.01726	0.15157
EGR1 (5)	*SLC12A8*	4.34	7.99	0.542	0.04185	0.23823
SIN3A (3)	*FAM192A*	20.31	30.48	0.666	0.01788	0.15157

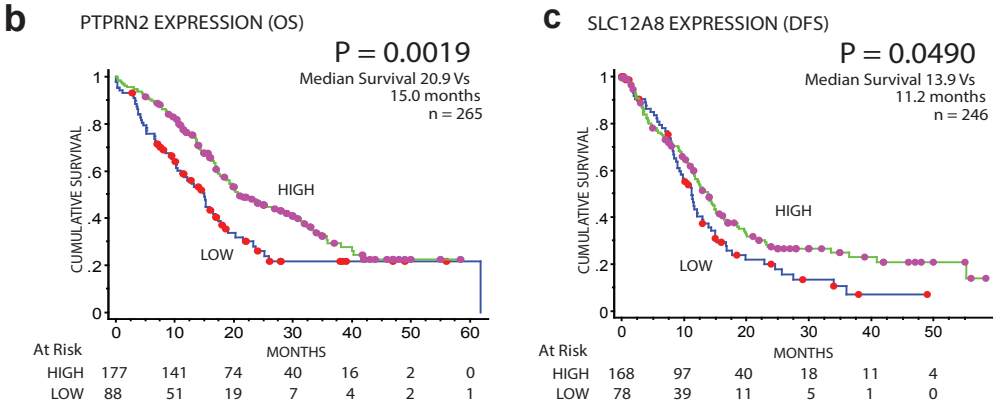

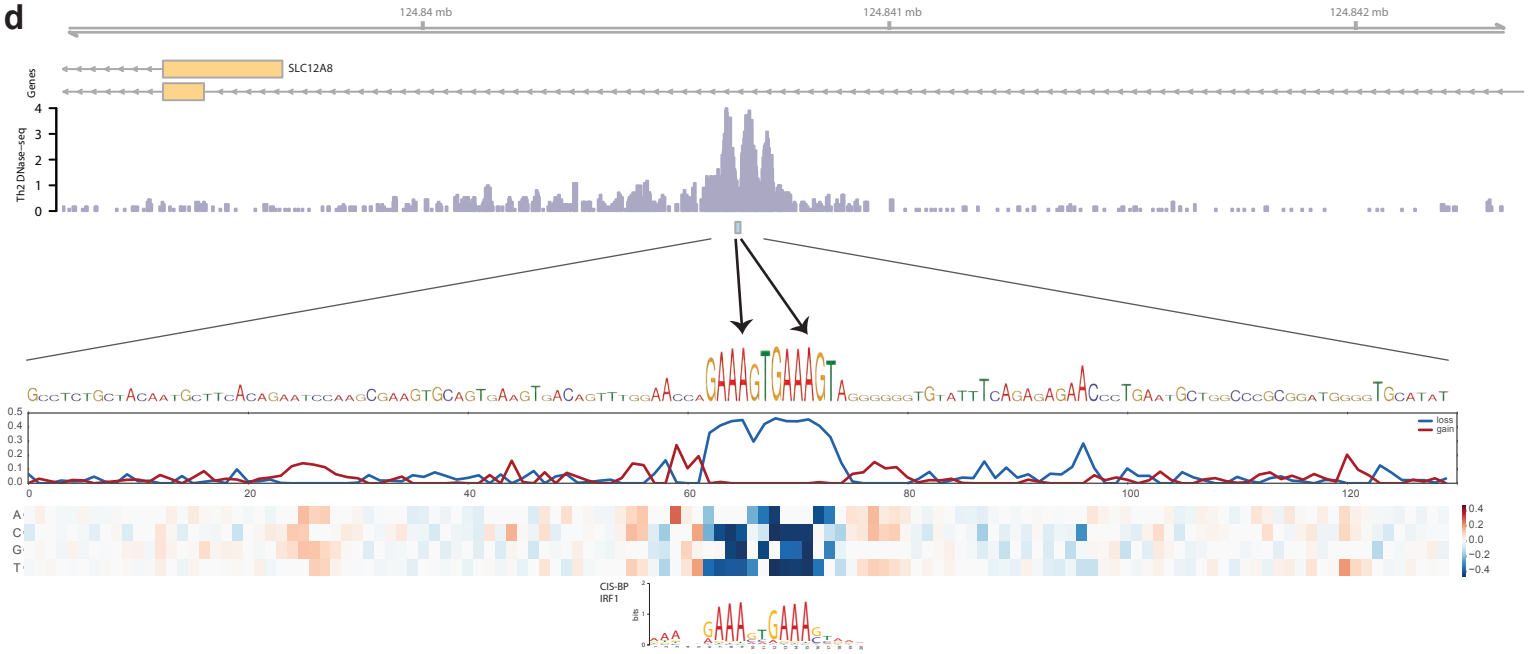

Figure 4 - Recurrent gene-proximal mutations correlate with gene expression changes in PDA.
(a) GECCO used gene expression data from matched PDA patients to correlate NCMs with changes in gene expression "Mut allele" = mean expression of linked gene in patients with associated CRR mutations. "WT allele" = mean expression of linked gene in patients without associated CRR mutations. **(b)** Analysis of overall survival (OS) in PDA patients expressing high (upper 2/3) and low (lower 1/3) levels of *PTPRN2*. Purple dots represent patients with high expression of *PTPRN2* "at risk" (alive). Red dots represent patients with low expression of *PTPRN2* "at risk" (alive). **(c)** Analysis of disease-free survival (DFS) in PDA patients expressing high (upper 2/3) and low (lower 1/3) levels of *SLC12A8*. **(d)** Two A→C mutations in a regulatory site on chromosome 3 at positions 124,840,671 and 124,840,678 alter critical nucleotides in an IRF1 and/or PRDM1 binding site. The regulatory site lies in an intron of one isoform and promoter of an alternative isoform of *SLC12A8*. At the bottom, heat map displays predicted change in accessibility, considered here as DNase-seq signal in GM12865. The line plots above measure the maximum (gain) and minimum (loss) predicted change; the loss highlights nucleotides that significantly alter the overall signal upon mutation as both of these mutations do.

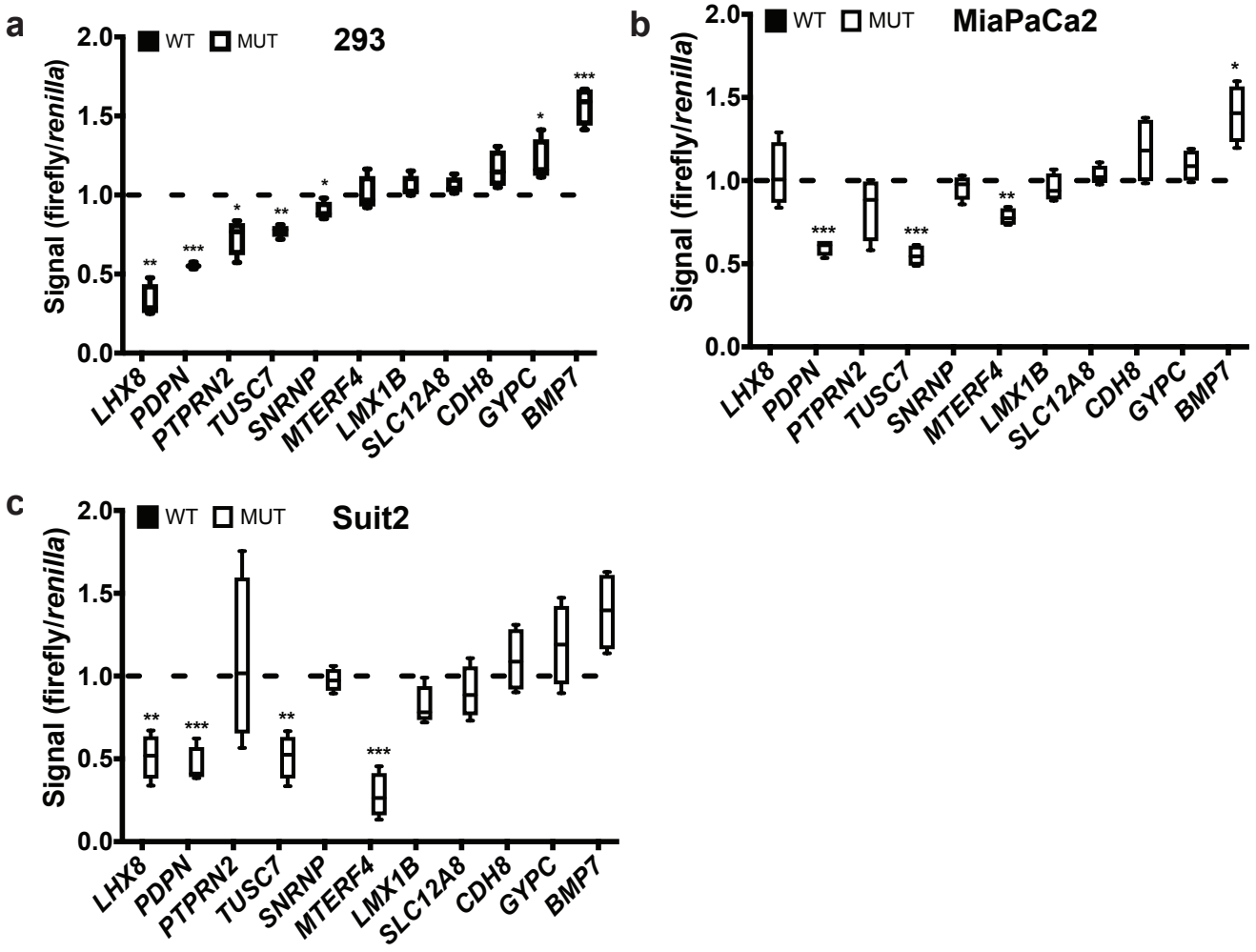

Figure 5 - Noncoding mutations modulate luciferase gene expression.
(a-c) Luciferase reporter assays of WT (black) and MUT sequences (white bars) are shown for selected NCMs associated with named genes. For each box-and-whisker plot, center line is the mean, box limits are min/max values, whiskers are standard error of the mean. (*, p<0.05; **, p<0.01; ***, p<0.001)

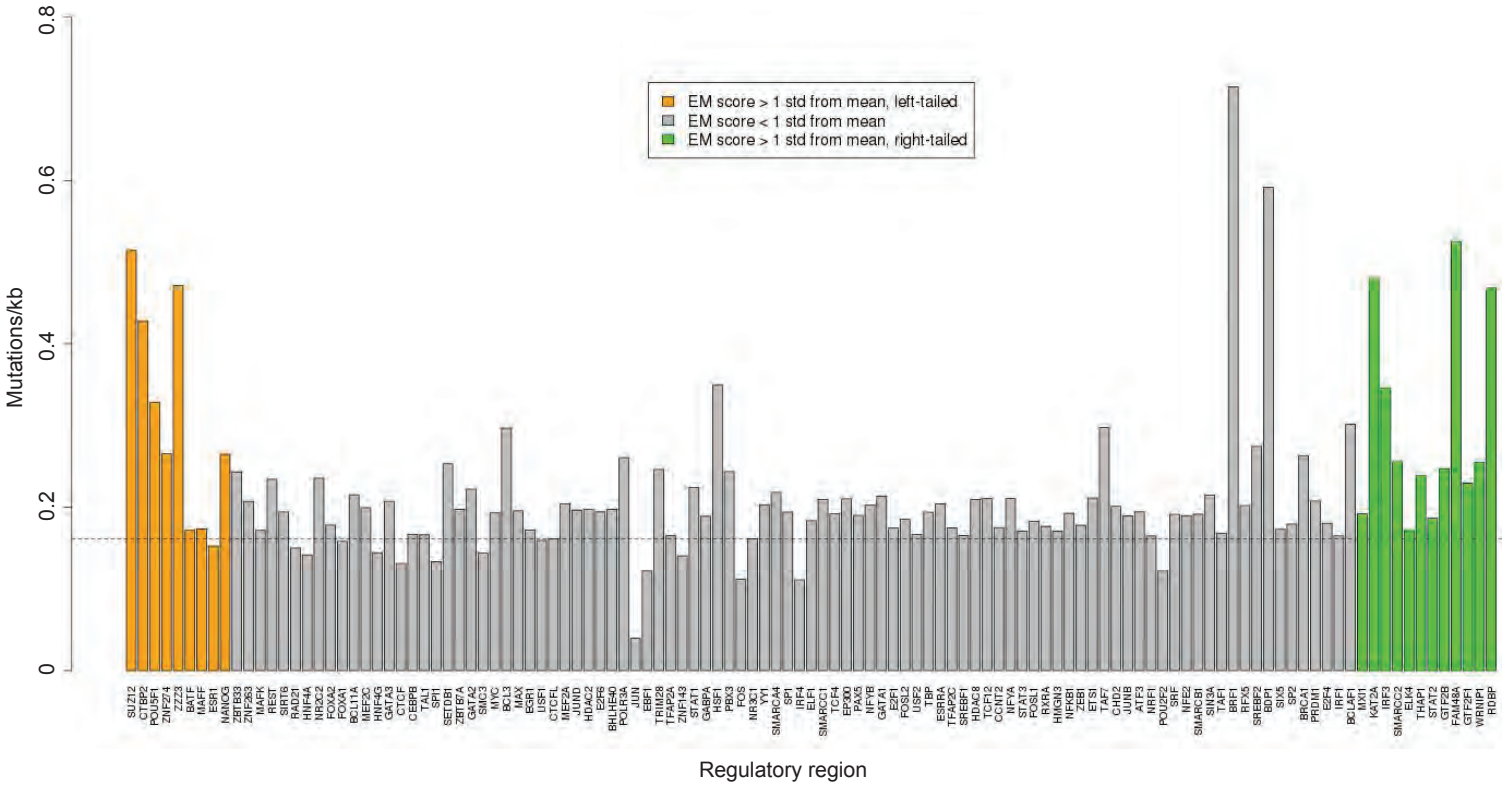

Figure 6 - Gene-proximal NCMs are enriched in specific classes of CRRs.
Percentage of CRRs with at least 2 mutations across the patient cohort, corrected for genome abundance and size, ordered from left to right by expression modulation score (EMS) (most repressive to most active). Dotted line represents mean mutation frequency across all CRRs.

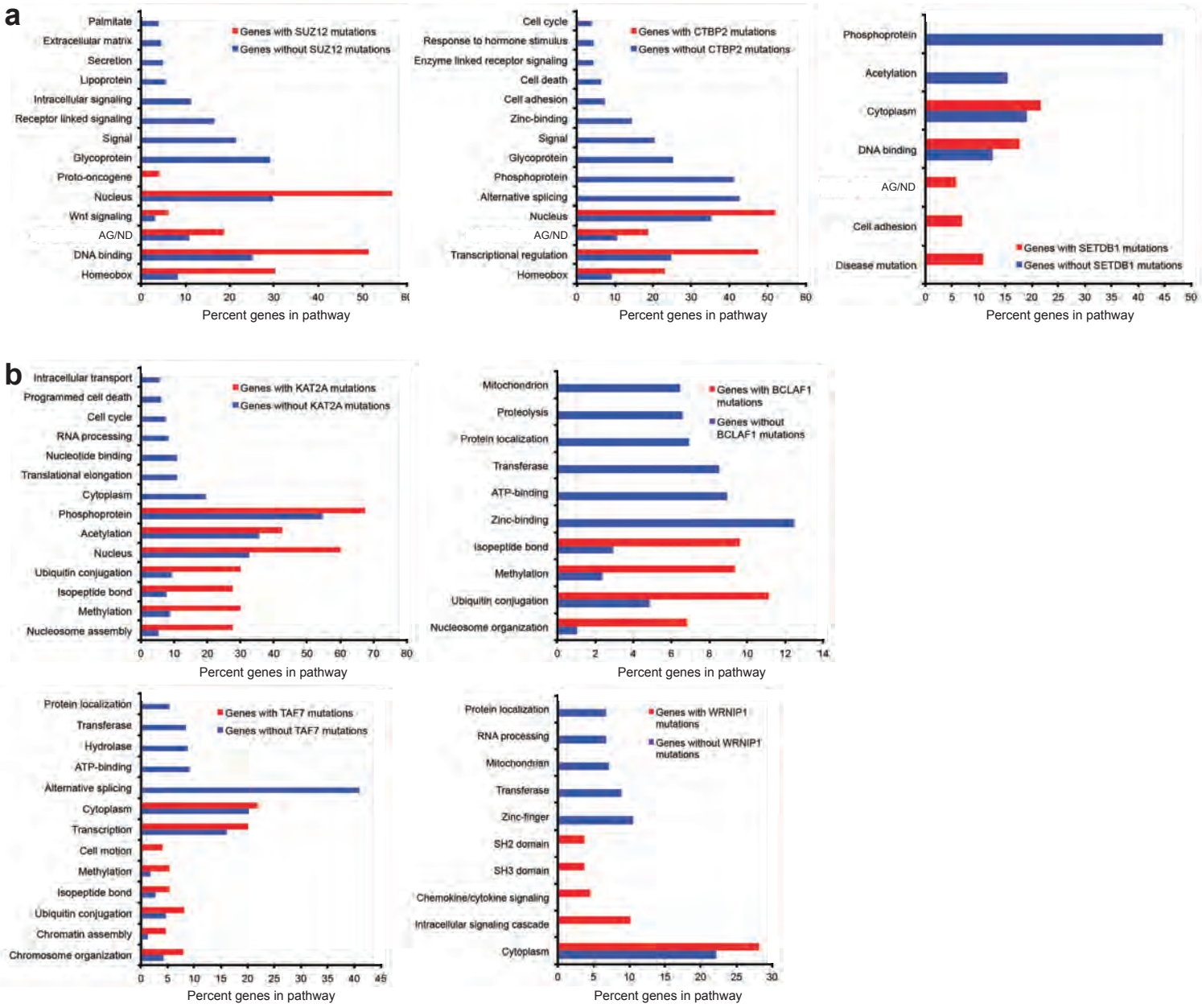

Figure 7 - Gene-proximal NCMs in repressors and activators cluster near distinct sets of genes. **(a)** Pathway analysis of genes associated with recurrently mutated repressive (SUZ12, CTBP2, SETDB1) sites (red bars), versus those never harboring NCMs in those CRRs (blue bars). **(b)** Pathway analysis of genes associated with recurrently mutated activator (KAT2A, BCLAF1, TAF7, WRNIP1) sites (red bars), versus those never harboring NCMs in those CRRs (blue bars). AG/ND, axon guidance/neuron differentiation.

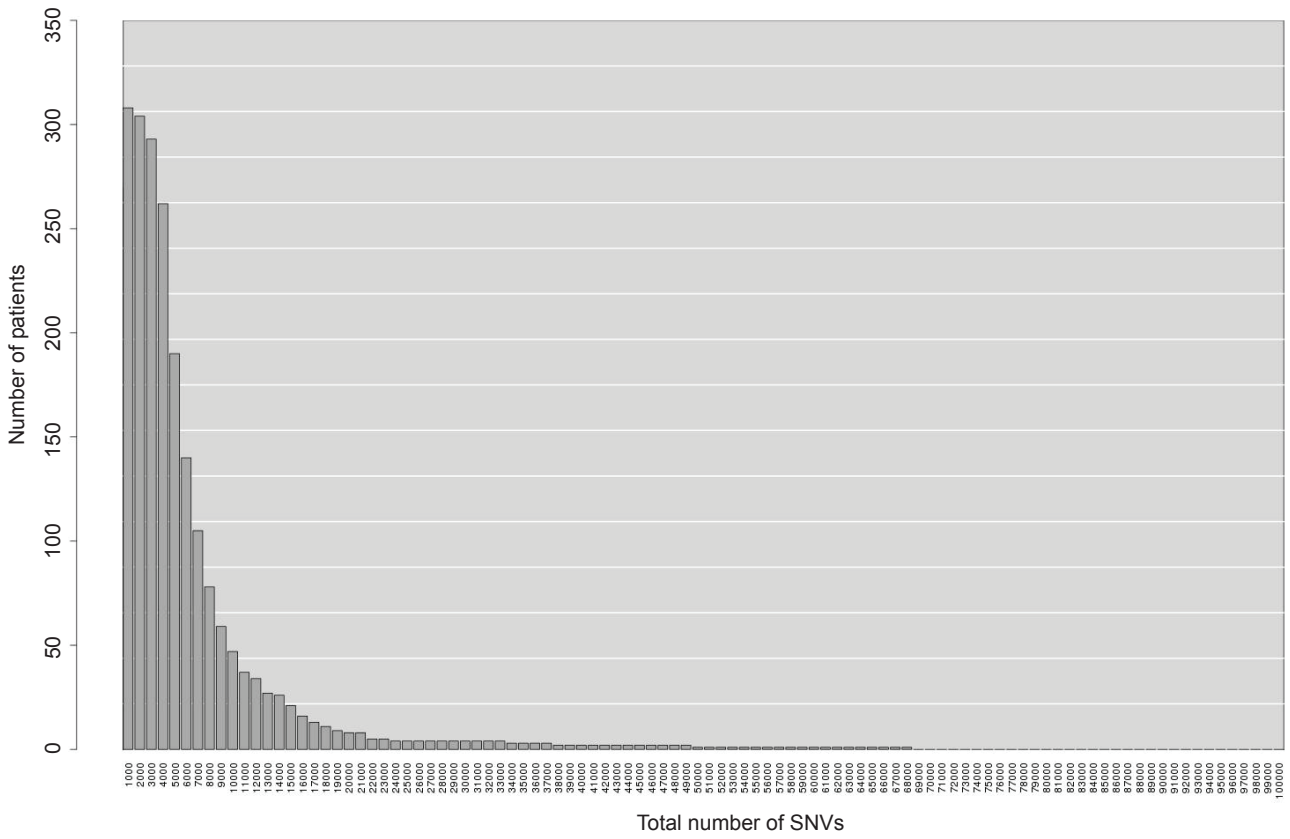

Supplementary Figure 1 - Identification of recurrent noncoding mutations in PDA.
Distribution of SNV rates across the patient cohort.

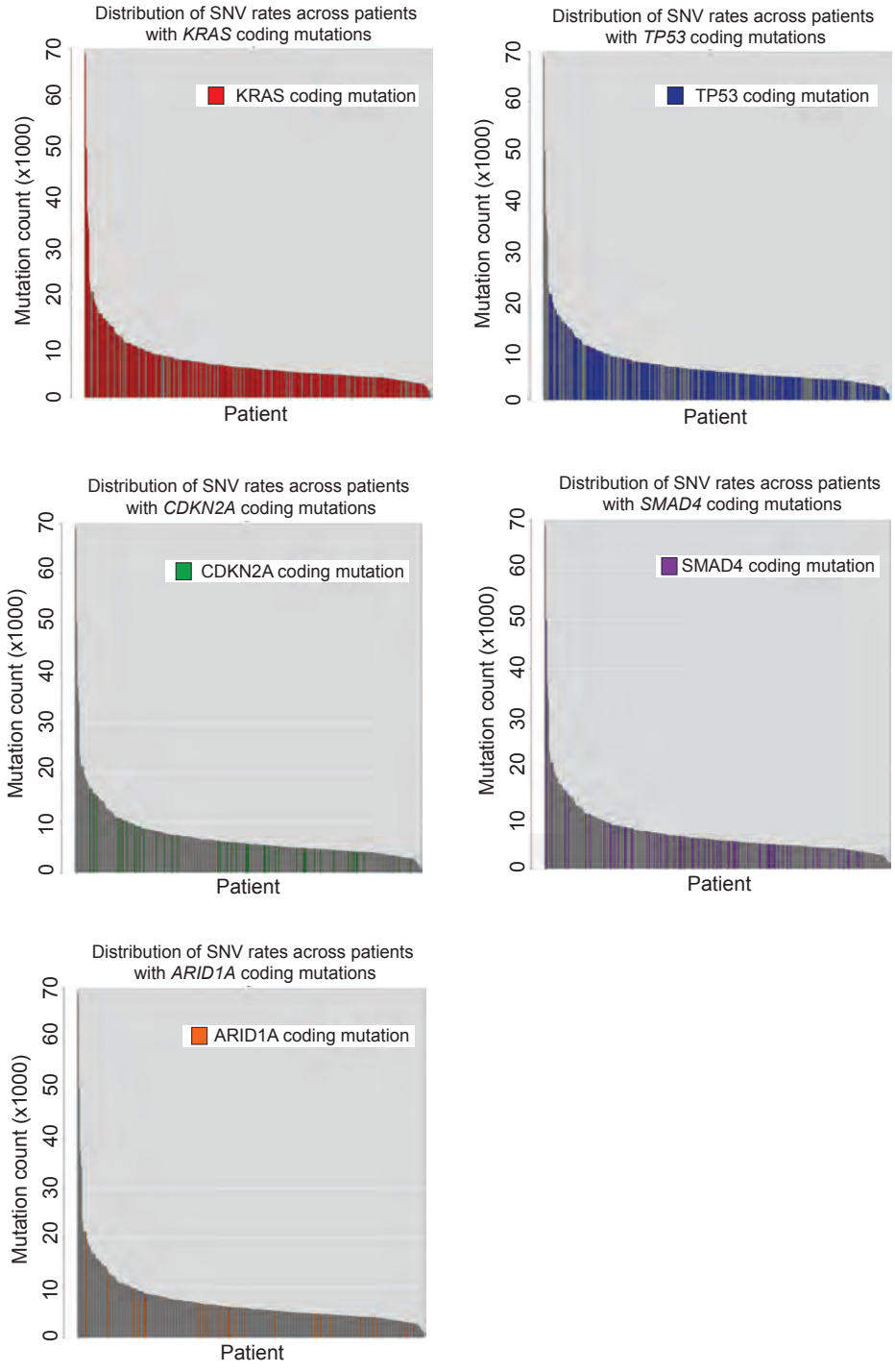

Supplementary Figure 2 - Overlap of SNVs and common coding mutations in PDA.
Distribution of SNVs across the patient cohort, with common coding mutations (colored bars) in PDA genes.

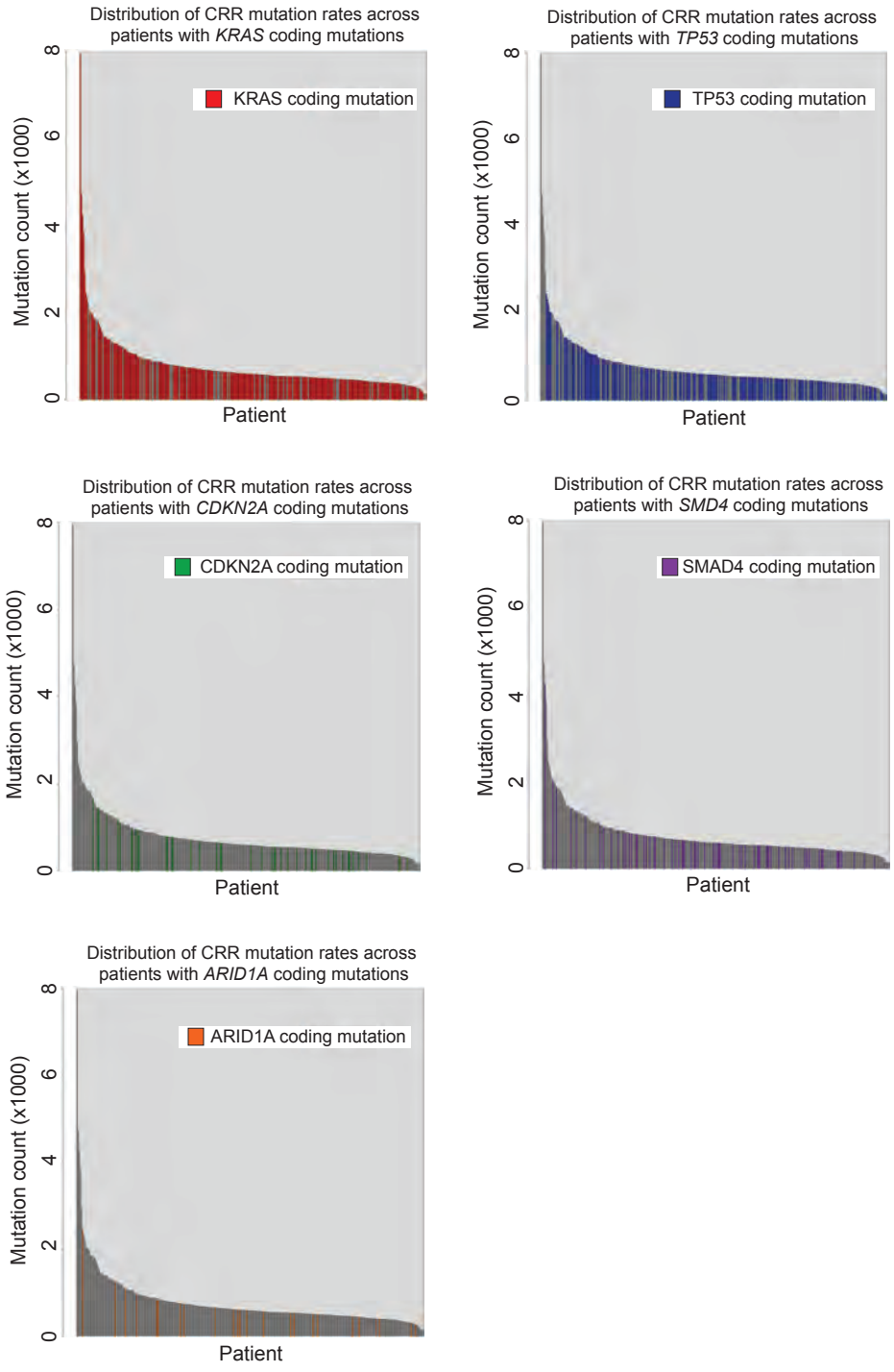

Supplementary Figure 3 - Overlap of gene-proximal NCMs in CRRs and common coding mutations in PDA. Distribution of CRR mutation rates across the patient cohort, with common coding mutations (colored bars) in PDA genes.

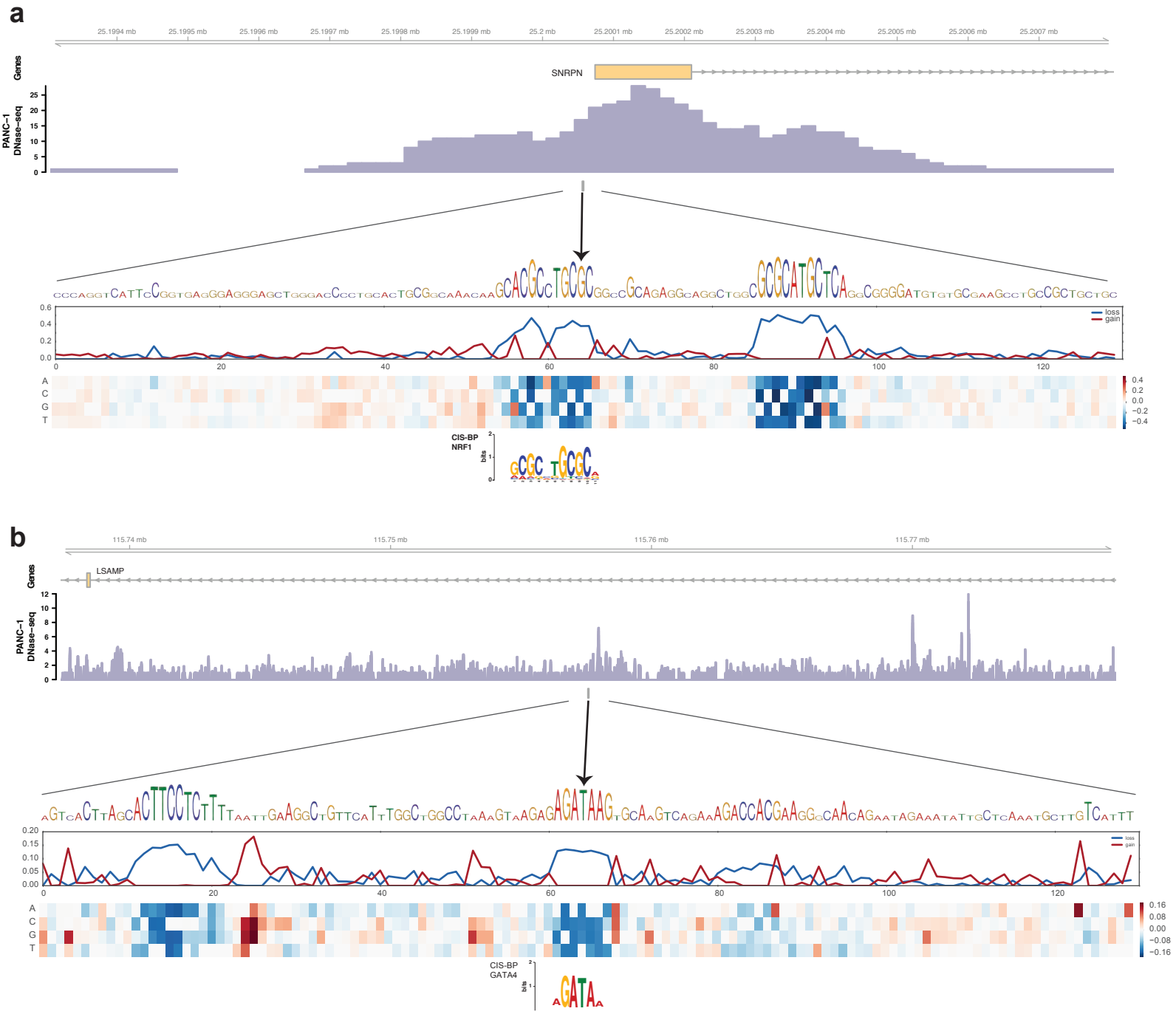

Supplementary Figure 4 - NCMs disrupt transcription factor binding motifs.
(a) A G→A mutation in a regulatory site on chromosome 15 at position 25,200,056 alters a critical nucleotide in an NRF1 binding site. The regulatory site lies in the promoter of *SNRPN*. At the bottom, the heat map displays the predicted change in binding, considered here as ChIP-seq signal for NRF1 in H1-hESCs. The line plots above measure the maximum (gain) and minimum (loss) predicted change; the loss highlights nucleotides that significantly alter the overall signal upon mutation as this mutation does. **(b)** A G->T mutation in a regulatory site on chromosome 3 at position 115,757,580 introduces a GATA factor binding site nearby an established PU.1 binding site. The heat map displays the predicted change in accessibility, considered here as DNase-seq signal in K562. In other cells, such as monocytes, the model predicts reduced accessibility, suggesting that GATA binding here may alter the combinatorial logic of the regulatory element in a complex fashion.

Genome-wide exactly recurrent (n≥6) noncoding mutations in PDA

Nearest gene	Patients (%)	Sequence	Gene name/protein function
COX7B2	7 (2.27)	GTCA(T)TA	cytochrome c oxidase subunit
OSBPL9	7 (2.27)	ATTA(T)AT	oxysterol binding protein-like 9; cholesterol transfer protein
WASF3	7 (2.27)	TTTT(A)AA	Wiskott-Aldrich syndrome protein family
ZNF81	7 (2.27)	AATA(T)AA	zinc finger protein; transcription factor
BNC2	6 (1.95)	TTTA(T)AA	basonuclin 2; zinc finger transcription factor
ELMO1	6 (1.95)	TTTA(T)AA	engulfment and cell motility 1; cytoskeletal rearrangement
GPR98	6 (1.95)	TCTC(A)TC	G protein-coupled receptor; central nervous system development
MYO16	6 (1.95)	GCTT(C)GC	myosin XVI; actin-based motor with ATPase activity
PDE3B	6 (1.95)	ATAG(T)AG	phosphodiesterase 3B; regulates cAMP binding of RAPGEF3
SOX5	6 (1.95)	ATAG(T)AG	SRY (sex determining region Y)-box 5; transcription factor
TMEM232	6 (1.95)	ATAG(T)AG	transmembrane protein 232

Supplementary Table 1 - Exactly recurrent mutations in PDA.
The most common exactly recurrent mutations across the patient cohort. Sequence of mutant allele in parenthesis.

NCM overlap with known PDA genes

PDA gene	CRR (# patients)
KRAS	-
TP53	-
CDKN2A	-
SMAD4	-
ARID1A	-
MLL3	-
PIK3CA	-
MAP2K4	-
BRAF	-
ZIM2	JUND (6)
PEG3	TAF1 (6), FOSL2 (5)
NEB	-
FLG	-
TGFBR2	-
ATM	-
HMCN1	-
ACVR1B	-
XIRP2	-
APC	-
FBXW7	-
RB1	-
USP47	-
BRCA2	-
PALB2	-
LKB1	-
PRSS1	-

Supplementary Table 2 - Distribution of gene-proximal NCMs near known PDA genes.
Analysis of the association of NCM clusters with known PDA genes.

Multivariate Analysis			
	Variable	**Hazard Ratio (95% CI)**	***P* Value**
A. Clinico-pathological and *PTPRN2* (n = 254, Starting model)	Sex (Male)	1.16 (0.83 – 1.62)	0.3933
	Lymph Node Metastases (Positive)	1.08 (0.65 – 1.81)	0.7561
	Grade (G3/4)	1.68 (1.19 – 2.38)	0.0033
	Tumor Size (> 20 mm)	1.90 (1.04 – 3.50)	0.0378
	Margin Involvement (Positive)	1.25 (0.87 – 1.81)	0.2208
	Tumor Location (Body/Tail)	1.71 (1.15 – 2.54)	0.0078
	Perineural Invasion (Positive)	1.48 (0.88 – 2.51)	0.1416
	Vascular Invasion (Positive)	1.65 (1.07 – 2.54)	0.0227
	PTPRN2 Expression (Low)	1.42 (1.00 – 2.01)	0.0505
B. Clinico-pathological and *PTPRN2* (Final model)	Grade (G3/4)	1.69 (1.21 – 2.38)	0.0021
	Tumor Size (> 20 mm)	1.98 (1.10 – 3.60)	0.0239
	Tumor Location (Body/Tail)	1.87 (1.26 – 2.75)	0.0017
	Vascular Invasion (Positive)	2.05 (1.44 – 2.92)	<0.0001
	PTPRN2 Expression (Low)	1.43 (1.00 – 2.02)	0.0453

Supplementary Table 3 - PTPRN2 multivariate analysis.
Multivariate analysis of clinico-pathological variables and PTPRN2 expression in the patient cohort.

CRR	EM Score	CRR	EM Score	CRR	EM Score
SUZ12	-0.686694944	HDAC2	0.150381608	RXRA	0.273722674
CTBP2	-0.674670553	E2F6	0.150409791	HMGN3	0.281526015
POU5F1	-0.56033248	BHLHE40	0.151537078	NFKB1	0.288817568
ZNF274	-0.245849532	POLR3A	0.159325596	ZEB1	0.303120139
ZZZ3	-0.161998971	JUN	0.162188074	ETS1	0.310574829
BATF	-0.135543815	EBF1	0.163190758	TAF7	0.313174867
MAFF	-0.075863388	TRIM28	0.163945818	CHD2	0.315050091
ESR1	-0.039131089	TFAP2A	0.164300299	JUNB	0.325497894
NANOG	-0.038471214	ZNF143	0.169254105	ATF3	0.326109056
ZBTB33	-0.030552156	STAT1	0.171479031	NRF1	0.326352606
ZNF263	-0.025572293	GABPA	0.172425715	POU2F2	0.327706868
MAFK	-0.02294752	HSF1	0.176973018	SRF	0.337389028
REST	-0.003580494	PBX3	0.177027193	NFE2	0.342471413
SIRT6	0.002156973	FOS	0.17863575	SMARCB1	0.345768127
RAD21	0.009059509	NR3C1	0.178665134	SIN3A	0.354604782
HNF4A	0.02493997	YY1	0.179418835	TAF1	0.363204782
NR2C2	0.030842166	SMARCA4	0.187416973	BRF1	0.364973559
FOXA2	0.035231355	SP1	0.189263356	RFX5	0.372691206
FOXA1	0.036020516	IRF4	0.189407346	SREBF2	0.380044338
BCL11A	0.040986649	ELF1	0.190484821	BDP1	0.396235351
MEF2C	0.046893332	SMARCC1	0.196306055	SIX5	0.402922065
HNF4G	0.047321602	TCF4	0.196772009	SP2	0.411373792
GATA3	0.056356258	EP300	0.198545703	BRCA1	0.420438253
CTCF	0.057809323	PAX5	0.199920331	PRDM1	0.421602184
CEBPB	0.069849107	NFYB	0.20623068	E2F4	0.421865085
TAL1	0.071199973	GATA1	0.207466124	IRF1	0.433584837
SPI1	0.085668185	E2F1	0.209186604	BCLAF1	0.433812837
SETDB1	0.093669622	FOSL2	0.220324569	MXI1	0.436922274
ZBTB7A	0.097578103	USF2	0.221126568	KAT2A	0.451063271
GATA2	0.098239781	TBP	0.227528399	IRF3	0.475299075
SMC3	0.103732676	ESRRA	0.230647673	SMARCC2	0.479021415
MYC	0.103926411	TFAP2C	0.231536652	ELK4	0.490643603
BCL3	0.112807799	SREBF1	0.240511397	THAP1	0.493514238
MAX	0.116546688	HDAC8	0.241186695	STAT2	0.524018361
EGR1	0.119910439	TCF12	0.251270827	GTF2B	0.544751967
USF1	0.120445295	CCNT2	0.263950123	FAM48A	0.567152197
CTCFL	0.129630002	NFYA	0.267597423	GTF2F1	0.669284919
MEF2A	0.130585096	STAT3	0.268609945	WRNIP1	0.693109157
JUND	0.132604078	FOSL1	0.268875227	RDBP	1.123049853

Supplementary Table 4 - CRR expression modulation scores.
Effect of CRR on activity of neighboring gene compared with all other genes in the genome (see Online Methods for analysis details). EM Score, expression modulation score.

Supplementary Note

Results

Somatic mutation calling

SNVs were called using BWA and GATK as previously described[1]. The rates and distribution of coding mutations in commonly mutated PDA genes (*KRAS*, *TP53*, *CDKN2A*, *SMAD4*, *ARID1A*) in the patient cohort was consistent with previous reports (**Supplementary Fig. 2**). We confirmed somatic status of the variants by searching for any evidence of the putative tumor variant in whole genome sequences of matched normal tissue for each patient.

Depletion of SNPs

Cancer mutations are depleted in accessible regulatory regions, particularly in those of the originating cell type[2]. Our set of SNPs was similarly depleted in DHSs from 164 cell types mapped by ENCODE and the Roadmap Epigenomics projects. The top ten most depleted DHS sets were from blood cells, for which >1.5 times fewer SNPs were present than after shuffling. Mapped cell types related to the pancreas were also depleted but inconspicuous in the broader context of many other cell types.

General feature of FunSeq2

The FunSeq2 pipeline filters cancer variants to exclude common polymorphisms from the 1000 Genomes project and retain those in noncoding regions. Further filters select for non-coding mutations in “sensitive” regions (those under strong negative selection), regions of high centrality in the protein-protein interaction network, ENCODE-defined regions captured by chromatin immunoprecipitation (ChIP), and mutations disrupting transcription factor binding motifs. We confirmed the somatic status of the mutations by comparing with matched normal DNA for each patient.

Enrichment of NCMs in CRRs

Noncoding mutations were found to be specifically enriched in certain classes of gene-proximal CRRs, including binding regions for the RNA Polymerase III Transcription Initiation Factors *BRF1* and *BDP1*, the Polycomb Repressive Complex 2 component *SUZ12*, the lysine acetyltransferase *KAT2A*, the negative elongation factor of RNA Polymerase II *RDBP*, and the transcriptional repressor *CTBP2*.

Discussion

The number of NCM-gene expression associations we uncover in this study is higher than that of similar whole genome cancer analyses. Several differences may account for this finding. First, we focused exclusively on a large number of samples from a single cancer type, rather than including a diverse array of cancers. As recurrent somatic NCMs are relatively uncommon (as are most coding mutations in PDA), reducing the heterogeneity of the samples allows detection of rare events. Second, we used GECCO to select those NCMs that are most likely to cause alterations in gene expression and focused on clusters of mutations within specific regulatory regions in close proximity to genes.

We provide evidence that NCMs in specific regulatory element classes are selected for during tumor evolution. These highly mutated regulatory element classes are predominantly those with the greatest impact on gene expression. Further research will

be required to uncover if these regions are actively promoting or repressing gene expression in PDA, or if they are independently associated with highly expressed or repressed genes.

Supplementary References

1. Waddell, N.*, et al.* Whole genomes redefine the mutational landscape of pancreatic cancer. *Nature* **518**, 495-501 (2015).
2. Polak, P.*, et al.* Cell-of-origin chromatin organization shapes the mutational landscape of cancer. *Nature* **518**, 360-364 (2015).